Escape and Capture on Halo Orbit Manifolds using Impulsive Maneuvers for Interplanetary Transfers: Applications to an Interplanetary Transportation System

Masaki Nakamiya

Doctor of Philosophy

Department of Space and Astronautical Science,

School of Physical Sciences,

The Graduate University for Advanced Studies, Japan

2008

ACKNOWLEDGMENTS

First of all, I would like to thank Prof. Makoto Yoshikawa of ISAS (Institute of Space and Astronautical Science) / JAXA (Japan Aerospace Exploration Agency), also affiliated with the Graduate University for Advanced Studies (Sokendai University), as one of my dissertation supervisors.

I would also like to express my appreciation to Prof. Hiroshi Yamakawa of Kyoto University, another supervisor of my dissertation, for providing advice and teaching.

I have gratitude to Prof. Daniel J. Scheeres of the University of Colorado at Boulder for welcoming me in the United States of America, and for providing valuable discussion and feedback about my research.

I would like to acknowledge my doctoral committee for giving comments and feedback on this work on this work.

I wish to express my thank to the Department of Space and Astronautical Science at the Graduate University for Advanced Studies (Sokendai University) for support of my research and my education, and would like to thank the members of Yoshikawa Lab seminar for helping me.

At last but not least, I thank my wife very much for her continuous support of my life.

ABSTRACT

Spacecraft escape and capture trajectories from/to Halo orbits of the L1 or L2 points using impulsive maneuvers at the periapsis of the manifolds for interplanetary transfers in the restricted Hill three-body problem were analyzed. This application is motivated by future proposals to place "deep space ports" at the Earth and Mars L1 or L2 points.

First, the feasibility of interplanetary trajectories between Earth Halo orbits and Mars Halo orbits was investigated, and such trajectories were designed with reasonable ΔV and flight time. Here, we utilized unstable and stable manifolds associated with the Halo orbits to approach the vicinity of the planet's surface, and assumed impulsive maneuvers for escape and capture trajectories from/to Halo orbits. Thus, characteristics of periapsis of unstable and stable manifolds were investigated. It was found that the stable and unstable manifolds of Halo orbits could intersect the surface of any of the planets of the solar system by changing the size of Halo orbits. At the same time, the time of flight for the escape and capture from/to Halo orbits using manifolds takes a long time generally. Therefore, reducing the time of flight for escape and the capture trajectories and linking Earth Halo orbits with Mars Halo orbit were discussed. Thereby, interplanetary trajectories between Earth and Mars Halo orbits with reasonable ΔV and flight time were found.

Next, applying to Earth-Mars transportation system using spaceports on Earth and Mars Halo orbits, we evaluated the system in terms of the spacecraft mass of round-trip transfer. As a result, the transfer between the low Earth orbits and the low Mars orbits via the planets' Halo orbit to leave propellant for the return could reduce the spacecraft wet mass compared with a direct round-trip transfer.

TABLE OF CONTENTS

CHAPTER 1

1 Introduction

1.1 Background

Since the start of the space age when Sputnik was launched by the former Soviet Union in 1957, there have been many space exploration missions to the Moon, Mars, Jupiter, and other solar system bodies with the goals of understanding the formation process of the solar system and the origin of life. Although most of them are one-way trip explorations that an instrumented spacecraft go to observe a target body, round-trip explorations such as the Hayabusa sample return mission are expected to increase in the future. Besides, for a human exploration to Mars, a round-trip transportation system is needed to carry and return people to/from Mars. However, it is difficult to construct the round-trip transportation system between Earth and target bodies because it needs large amount of propellant. In fact, the massive Saturn V rocket was required for the launch to carry the return propellant to the moon in the Apollo program. Therefore, in order to establish a round-trip interplanetary transportation system, it is cost effective for a reduction of spacecraft mass to leave the return propellant at some places on the way to a target body. Thus, there has been great interest in the vicinity of libration points (L1/L2) as candidate locations for such a relay point for transportation.

The libration points of the Circular Restricted 3-Body Problem (CR3BP) are located where the gravity of the primary and secondary bodies and centrifugal force are balanced. In particular, the position of L1 and L2, which lie on the line connecting the two bodies, can be considered equivalent to the boundary of the gravitational dominance of the secondary body. Thus, a transfer to the inner or outer planets is relatively simple by addition of energy to a spacecraft in the vicinity of the L1 and L2 points. Actually, these points are considered as candidate gateways for interplanetary transfers in the future. Lo and Ross studied the use of the Earth-Moon L1 point as the staging node for further human expeditions [9,10]. Farquhar described a plan to use the Sun-Earth L2 libration point as the primary hub for future human space activities in the Earth's neighborhood [11,12]. The Japan Aerospace Exploration Agency (JAXA) has started investigating a deep space port built in the vicinity of the L2 point of the Sun-Earth system [13]. Recently, the analysis and design

of transfer orbits using invariant manifolds associated with periodic orbits around the libration points have been a topic of study [14-20]. The escape trajectories from the libration points of Sun-Earth system have also been examined [21-23]. Moreover, these L1 and L2 points are also notable location for astronomical observatories because an object around these points can maintain the same position with respect to the two bodies. Therefore, transfers between the secondary body and the libration point have been investigated extensively in the past [1-6]. In fact, starting with the ISEE-3 (International Sun–Earth Explorer-3) launched in 1978, several astronomical satellites such as the SOHO (Solar and Heliospheric Observatory), WMAP (Wilkinson Microwave Anisotropy Probe), Genesis, and so on have already utilized such locations around the L1 and L2 points of the Sun-Earth system [7]. From now, large astronomical observatories like the JWST (James Webb Space Telescope), Plank, Herschel and SPICA (SPace Infrared Telescope for Cosmology and Astrophysics) will likely be located near the Sun Earth L2 point [8]. The early libration astronomy missions have not been designed for human servicing and repair, but future libration missions will probably require some level of servicing and repair by people. For human access to the L1/L2 points, putting spaceports at L1/L2 points in the future is to be expected.

Furthermore, if spaceports are built around not only the Sun-Earth but Sun-Target planet L1/L2 points, we can separate the transportation system into three regions: transfer inside the gravity field of the Earth, transfer inside the gravity field of a target planet, and the interplanetary transfer phase as shown in Fig. 1.1 [11]. Moreover, assuming that propellants are left at these spaceports on the way to the target planet, the mass of spacecraft could be reduced. Therefore, the system using spaceports as relay points facilitates round-trip exploration and also leads to a reusable transportation system [8,10]. In the past, capture trajectories to the secondary body in the three-body problem were studied [24-29]. However, capture trajectories from interplanetary transfers to Halo orbits of target bodies, and also interplanetary transfers between Halo orbits are not fully understood. Alonso & Howell studied interplanetary transfers between Halo orbits with deep space impulsive maneuvers using manifolds to move toward outer space from Halo orbits directly without approaching planet in the vicinity of the planet once [41]. In this study, interplanetary transfers between Halo orbits are investigated, assuming a new way to use manifolds to approach the vicinity of the planet's surface and to perform impulsive maneuvers at periapsis near the surface of planets for interplanetary transfers. And

finally, an application to Earth-Mars transportation system using spaceports at Earth and Mars Halo orbits is discussed.

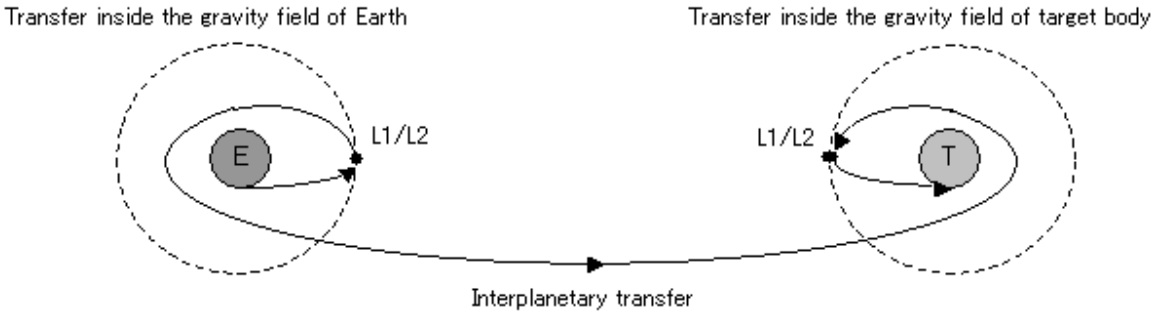

Figure 1.1: Vision of an interplanetary transfer in the future.

1.2 Overview of the Dissertation

The objectives of this dissertation are as follows:

1. to analyze spacecraft escape and capture impulsive trajectories from/to Halo orbits.
2. to reduce the time of flight for escape/capture trajectories from/to Halo orbits.
3. to examine linking interplanetary transfer trajectories with Halo stable/unstable manifolds, with an Earth-Mars transportation system as a case study.

In order to present these goals, this dissertation is divided into 6 chapters:

CHAPTER 2: In this chapter, the dynamics of the Hill three-body problem is described. Moreover, the local motions near the L1 and L2 points are shown.

CHAPTER 3: Escape and capture trajectories from/to Halo orbits using impulsive maneuver at periapsis of invariant manifolds are defined. The characteristics of the periapsis of manifolds are then investigated.

CHAPTER 4: Reducing the time of flight for escape and capture trajectories are discussed based on using stable manifolds.

CHAPTER 5: Connecting interplanetary trajectories with stable/unstable manifolds of Halo orbits are analyzed.

CHAPTER 6: Our study of the escape and capture impulsive trajectories from/to Halo orbit are applied to an Earth-Mars transportation system. The round-trip Earth Mars transportation system using Halo orbits is then evaluated in terms of the required spacecraft wet mass.

CHAPTER 7: Finally, the summary and conclusions are presented.

CHAPTER 2

2 Hill Three-Body Problem

The physical model considered in this paper is the restricted Hill three-body model. This model is a simplified case of the Circular Restricted 3-Body Problem (CR3BP) and describes the dynamics of a massless particle attracted by two point masses revolving around each other in a circular obit (see Fig. 2.1). In fact, the Hill model can be obtained from the CR3BP by setting the origin of the coordinate system to be at the secondary body, and then assuming that the distance of the satellite from the origin is small compared to the distance between the target body and the Sun. The resulting equations of motion provide a good description for the motion of a spacecraft in the vicinity of the L1 and L2 libration points of the secondary body [30].

2.1 From the CR3BP to Hill Three-Body Problem [31,32]

Let m_1 and m_2 be the masses of the primary and secondary body, respectively, with the bodies following circular orbits around their common center of mass, having a constant distance, D, distance between them. The circular restricted three-body problem assumes that the mass of the third body is negligible. In a rotating frame with origin at the center of mass, the equations of motion for the massless particle (spacecraft), which does not disturb the motion of primary and secondary bodies, are given by

$$\ddot{X} - 2\omega\dot{Y} = \omega^2 X - \mu_1 \frac{X+\mu D}{R_1^3} - \mu_2 \frac{X-(1-\mu)D}{R_2^3}, \tag{2.1}$$

$$\ddot{Y} + 2\omega\dot{X} = \omega^2 Y - \mu_1 \frac{Y}{R_1^3} - \mu_2 \frac{Y}{R_2^3}, \tag{2.2}$$

$$\ddot{Z} = -\mu_1 \frac{Z}{R_1^3} - \mu_2 \frac{Z}{R_2^3}, \tag{2.3}$$

where $\mu_1 = Gm_1$ and $\mu_2 = Gm_2$ are the gravitational parameter of the two bodies, and $\mu = m_2/(m_1+m_2)$ is a mass ratio. Moreover, $R_1 = \sqrt{(X+\mu D)^2 + Y^2 + Z^2}$ and $R_2 = \sqrt{(X-(1-\mu)D)^2 + Y^2 + Z^2}$ are the

distances from the center of the primary and the secondary bodies to the spacecraft, respectively, and ω is the angular velocity of the secondary body about the primary body. The positions of the bodies are *(-μD*, 0) and (*(1-μ)D*, 0). The terms $2\omega\dot{Y}$ and $2\omega\dot{X}$ are the Coriolis accelerations, and $\omega^2 X$ and $\omega^2 Y$ are centrifugal acceleration terms.

The equations of motion, given by Equations (2.1), (2.2), and (2.3), for the circular restricted three-body problem can also be expressed in terms of a pseudo-potential $\Omega^* = \Omega^*(X, Y, Z)$ as follows:

$$\ddot{X} - 2\omega\dot{Y} = \frac{\partial \Omega^*}{\partial X} = \Omega_X^* \quad , \tag{2.4}$$

$$\ddot{Y} + 2\omega\dot{X} = \frac{\partial \Omega^*}{\partial Y} = \Omega_Y^* \quad , \tag{2.5}$$

$$\ddot{Z} = \frac{\partial \Omega^*}{\partial Z} = \Omega_Z^* \quad , \tag{2.6}$$

where the pseudo-potential, Ω^*, is in fact the centrifugal plus gravitational force potential, defined as

$$\Omega^*(X, Y, Z) = \frac{1}{2}\omega^2 (X^2 + Y^2) + \frac{\mu_1}{R_1^3} + \frac{\mu_2}{R_2^3} \tag{2.7}$$

To study the motion in the vicinity of the small secondary body, the origin of the coordinate system is transferred to the secondary body, and the coordinates are scaled by a factor $\mu^{1/3}$. Thus, they become

$$X - (1-\mu)D = \mu^{1/3} x\,,\ Y = \mu^{1/3} y\,, \text{ and } Z = \mu^{1/3} z \tag{2.8}$$

When Equations (2.8) are introduced in the equations of motion (2.1) - (2.3), assuming that the secondary body is very small, that is μ is small, and after dividing by $\mu^{1/3}$,

$$\ddot{x} - 2\omega\dot{y} = 3\omega^2 x - \frac{\mu_2}{r^3} x \quad , \tag{2.9}$$

$$\ddot{y} + 2\omega\dot{x} = -\frac{\mu_2}{r^3} y \quad , \tag{2.10}$$

$$\ddot{z} = -\omega^2 z - \frac{\mu_2}{r^3} z \quad , \tag{2.11}$$

where $r = \sqrt{x^2 + y^2 + z^2}$ is the distance from the center of the second smaller body to the spacecraft.

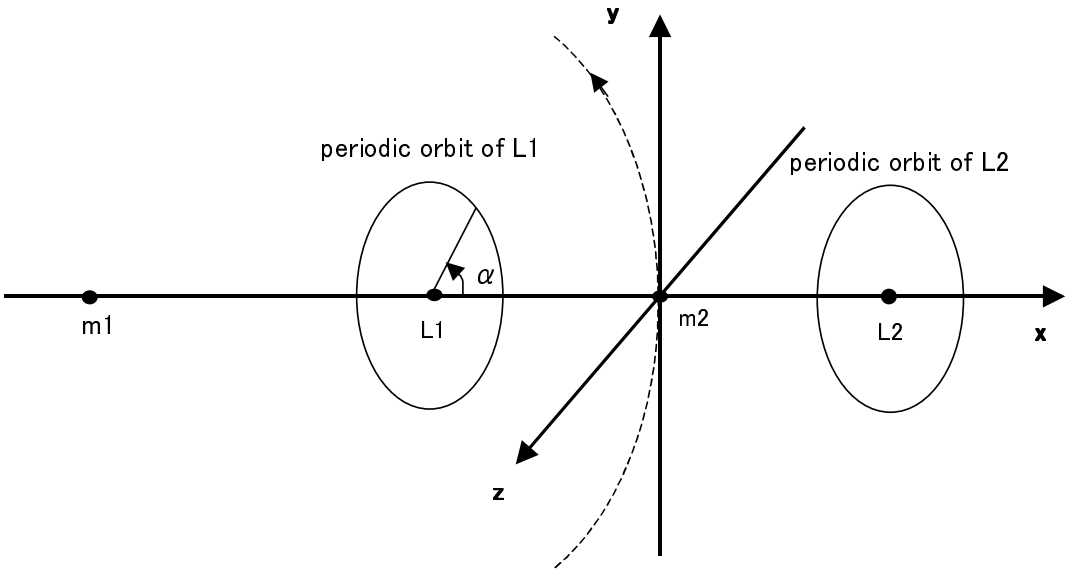

Figure 2.1: Geometry of the restricted Hill three-body model.

2.2 Libration Points

In the circular restricted 3-body problem model there are five points where the gravity of the primary and secondary bodies and centrifugal force acting on S/C are balanced, which are called libration points. These libration points are defined by the conditions

$$\dot{x} = \dot{y} = \dot{z} = 0 \text{ and } \ddot{x} = \ddot{y} = \ddot{z} = 0 \tag{2.12}$$

for which reason the points are called equilibrium points. From these equations, we can find the two collinear libration points of interest (L1 and L2) in the restricted Hill three-body problem

$$x = \pm\left(\mu/3\omega^2\right)^{1/3}, y = z = 0\,. \tag{2.13}$$

and they are symmetric to the origin with coordinates.

2.3 Jacobi Integral

The restricted Hill three-body problem has an integral of motion similar to the CR3BP. Adding equations (2.9) - (2.11) after multiplying them by $\dot{x}, \dot{y}, \text{and } \dot{z}$, respectively, we obtain

$$\ddot{x}\dot{x} + \ddot{y}\dot{y} + \ddot{z}\dot{z} = 3\omega^2 \dot{x}x - \omega^2 \dot{z}z - \frac{\mu}{r^3}(\dot{x}x + \dot{y}y + \dot{z}z). \tag{2.14}$$

Which, after integration, becomes,

$$J = \frac{1}{2}v^2 - \frac{\mu}{r} + \frac{1}{2}\omega^2\left(3x^2 - z^2\right), \tag{2.15}$$

where $v = \sqrt{\dot{x}^2 + \dot{y}^2 + \dot{z}^2}$ is the velocity of the particle in the rotating frame, *J* is a constant called *the Jacobi integral (Jacobi constant)*, which is a conservative quantity determined from the initial conditions. The value of this constant has a strong influence on the dynamics of motion. The condition $v^2 \geq 0$ in Eq. (2.15) impose a restriction on the allowable position for the motion at any given value of *J*. Setting $v = 0$ defines the zero-velocity surface, which sets a physical boundary of the allowable motion at a given value of *J*. In particular, the critical value of *J* at L1 and L2 defines the energy at which the zero-velocity surfaces open at L1 and L2, and is expressed as:

$$J_{L1,2} = -\frac{1}{2}(9\mu\omega)^{2/3} \tag{2.16}$$

2.4 Normalization

Next, we normalize the above equations setting the unit length and the unit time as follows:

$$l = \left(\frac{\mu}{\omega^2}\right)^{1/3} \text{ and } \tau = \frac{1}{\omega}. \tag{2.17}$$

The normalized equations of motion (2.9)- (2.11) are then

$$\ddot{x} - 2\dot{y} = 3x - \frac{x}{r^3}, \tag{2.18}$$

$$\ddot{y} + 2\dot{x} = -\frac{y}{r^3}, \tag{2.19}$$

$$\ddot{z} + z = -\frac{z}{r^3} \quad . \tag{2.20}$$

This normalization allows us to eliminate all free parameters from the equations. Thus, computations performed for them can be scaled to any physical system by multiplying by the unit length and time, which only depend on the properties of the primary and secondary bodies. We may introduce again a pseudo-potential function

$$\Omega(x, y, z) = \frac{1}{2}(3x^2 - z^2) + \frac{1}{r} + \mu^{1/3} x\left(x^2 - \frac{3}{2}(y^2 + z^2)\right) + \mathrm{O}(\mu^{2/3}) \tag{2.21}$$

and so the equations of motion (2.18)-(2.20) may be written as

$$\ddot{x} - 2\dot{y} = \frac{\partial \Omega}{\partial x} = \Omega_x \quad , \tag{2.22}$$

$$\ddot{y} + 2\dot{x} = \frac{\partial \Omega}{\partial y} = \Omega_y \quad , \tag{2.23}$$

$$\ddot{z} = \frac{\partial \Omega}{\partial z} = \Omega_z \quad . \tag{2.24}$$

Moreover, this normalization is equivalent to $\omega = 1$ and $\mu = 1$, thus, the normalized x coordinate of libration points and the normalized value of J at L1 and L2 are equal to

$$x_{L1,2} = \pm(1/3)^{1/3} = \pm 0.693... \tag{2.25}$$

$$J_{L1,2} = -\frac{1}{2} 9^{2/3} = -2.16337... \tag{2.26}$$

Table 2.1 gives the normalized radius for the planets of the solar system. This is a quantity of interest as it defines the closest periapsis passage possible to the planet, and defines the periapsis radius where significant drag forces are available for an aerocapture spacecraft.

Table 2.1 Normalized Radius of the Solar System Planet

Planet	Mass, $[\text{kg} \times 10^{23}]$	Gravitational parameter, $[\text{km}^3/\text{s}^2 \times 10^5]$	Mean motion, $[\text{rad/s} \times 10^{-7}]$	Normalized radius
Mercury	0.3302	0.220329	8.27	0.007663
Venus	4.869	3.248889	3.24	0.00415
Earth	5.9742	3.986345	1.99	0.002955
Mars	0.64191	0.428321	1.06	0.002173
Jupiter	1899	1267.127	0.168	0.000933
Saturn	568.8	379.5375	0.0676	0.000641
Uranus	86.86	57.9582	0.0267	0.000253
Neptune	102.4	68.32742	0.0121	0.000148

2.5 Linearized Equation of Motion around L1/L2 Points

In order to study the motion near the L1 and L2 equilibrium points, let

$$x = x_{L1,2} + \xi, \quad y = y_{L1,2} + \eta, \quad z = z_{L1,2} + \zeta \quad , \tag{2.27}$$

where $(x_{L1,2}, y_{L1,2}, z_{L1,2})$ are the coordinates of the L1 and L2 points and (ξ, η, ζ) are the components of the position vector of the spacecraft relative to the L1/L2 points. The function Ω may be expanded around L1/L2 point, giving

$$\begin{aligned}\Omega = {} & \Omega(x_{L1,2}, y_{L1,2}, z_{L1,2}) + \Omega_x(x_{L1,2}, y_{L1,2}, z_{L1,2})\xi + \Omega_y(x_{L1,2}, y_{L1,2}, z_{L1,2})\eta + \Omega_z(x_{L1,2}, y_{L1,2}, z_{L1,2})\zeta \\ & + \frac{1}{2!}\Omega_{xx}(x_{L1,2}, y_{L1,2}, z_{L1,2})\xi^2 + \frac{1}{2!}\Omega_{yy}(x_{L1,2}, y_{L1,2}, z_{L1,2})\eta^2 + \frac{1}{2!}\Omega_{zz}(x_{L1,2}, y_{L1,2}, z_{L1,2})\zeta^2 \\ & + \Omega_{xy}(x_{L1,2}, y_{L1,2}, z_{L1,2})\xi\eta + \Omega_{yz}(x_{L1,2}, y_{L1,2}, z_{L1,2})\eta\zeta + \Omega_{zx}(x_{L1,2}, y_{L1,2}, z_{L1,2})\zeta\xi + \mathrm{O}(3).\end{aligned} \tag{2.28}$$

The differential equations of motion (2.13)-(2.15) become

$$\begin{aligned}\ddot{\xi} - 2\dot{\eta} &= \Omega_{xx}\big|_{L1,2}\xi + \Omega_{xy}\big|_{L1,2}\eta + \Omega_{xz}\big|_{L1,2}\zeta + \mathrm{O}(2) \\ &\cong \Omega^0_{xx}\xi + \Omega^0_{xy}\eta + \Omega^0_{xz}\zeta\end{aligned} \quad , \tag{2.29}$$

$$\begin{aligned}\ddot{\eta} + 2\dot{\xi} &= \Omega_{yx}\big|_{L1,2}\xi + \Omega_{yy}\big|_{L1,2}\eta + \Omega_{yz}\big|_{L1,2}\zeta + \mathrm{O}(2) \\ &\cong \Omega^0_{yx}\xi + \Omega^0_{yy}\eta + \Omega^0_{yz}\zeta\end{aligned} \quad , \tag{2.30}$$

$$\ddot{\zeta} = \Omega_{zx}\Big|_{L1,2}\xi + \Omega_{zy}\Big|_{L1,2}\eta + \Omega_{zz}\Big|_{L1,2}\zeta + \mathrm{O}(2)$$
$$\cong \Omega^0_{zx}\xi + \Omega^0_{zy}\eta + \Omega^0_{zz}\zeta \quad , \tag{2.31}$$

where the symbols *O(2)* and *O(3)* stand for second-order term in ξ, η and ζ. $\Omega_x\Big|_{L1,2} = \Omega_y\Big|_{L1,2} = \Omega_z\Big|_{L1,2} = 0$ since L1 and L2 are the equilibrium points. Moreover, since the L1 and L2 points are always on the *x*-axis, i.e., $y_{L1,2} = z_{L1,2} = 0$. Therefore, $\Omega^0_{xy} = \Omega^0_{yx} = \Omega^0_{xz} = \Omega^0_{zx} = \Omega^0_{yz} = \Omega^0_{zy} = 0$. Then, for the L1 and L2 points, equations (2.29)-(2.31) are simplified to

$$\ddot{\xi} - 2\dot{\eta} = \Omega^0_{xx}\xi \quad , \tag{2.32}$$

$$\ddot{\eta} + 2\dot{\xi} = \Omega^0_{yy}\eta \quad , \tag{2.33}$$

$$\ddot{\zeta} = \Omega^0_{zz}\zeta \quad . \tag{2.34}$$

The in-plane characteristic equation associated with equations (2.32) and (2.33) is of the form

$$\lambda^4 + (4 - \Omega^0_{xx} - \Omega^0_{yy})\lambda^2 + \Omega^0_{xx}\Omega^0_{yy} = 0 \quad , \tag{2.35}$$

and the in-plane eigenvalues can be expressed as

$$\lambda_{1,2} = \pm\sqrt{-\beta_1 + \sqrt{\beta_1^2 + \beta_2^2}} = \pm\sigma \quad , \tag{2.36}$$

$$\lambda_{3,4} = \pm j\sqrt{\beta_1 + \sqrt{\beta_1^2 + \beta_2^2}} = \pm j\omega_{xy} \quad , \tag{2.37}$$

where $\beta_1 = 2 - (\Omega^0_{xx} + \Omega^0_{yy})/2$ and $\beta_2 = -\Omega^0_{xx}\Omega^0_{yy} > 0$, and j is the imaginary unit. Additionally ω_{xy} is called the nondimensional frequency of the in-plane oscillatory mode.

The out-of-plane characteristic equation associate with equation (2.34) is

$$\lambda^2 - \Omega^0_{zz} = 0 \quad , \tag{2.38}$$

and the out-of-plane eigenvalues are

$$\lambda_{5,6} = \pm j\sqrt{|\Omega_{zz}^0|} = \pm j\omega_z \quad , \tag{2.39}$$

where ω_z is called the nondimensional frequency of the out-of-plane oscillatory mode.

At L1 and L2 points in the Hill model, we have

$$\Omega_{xx}^0 = 9, \quad \Omega_{yy}^0 = -3, \quad \Omega_{zz}^0 = -4 \quad , \tag{2.40}$$

and the eigenvalues are

$$\lambda_{1,2} = \pm\sigma \cong \pm 2.508 \quad , \tag{2.41}$$

$$\lambda_{3,4} = \pm j\omega_{xy} = \pm j2.072 \quad , \tag{2.42}$$

$$\lambda_{5,6} = \pm j\omega_z = \pm j2 \quad . \tag{2.43}$$

The general solutions for ξ and η are

$$\xi = \sum_{i=1}^{4} A_i e^{\lambda_i t} \quad , \tag{2.44}$$

$$\eta = \sum_{i=1}^{4} B_i e^{\lambda_i t} \quad , \tag{2.45}$$

where A_i and B_i are constant, but not independent. Direct substitution of equations (2.44)-(2.45) into equations (2.32)-(2.33) results in the following relation between A_i and B_i, that is,

$$B_i = \frac{\lambda_i^2 - \Omega_{xx}^0}{2\lambda_i} A_i = \alpha_i A_i \quad , \tag{2.46}$$

.

and at the initial time,

$$\xi_0 = \sum_{i=1}^{4} A_i e^{\lambda_i t_0} \quad , \tag{2.47}$$

$$\dot{\xi}_0 = \sum_{i=1}^{4} \lambda_i A_i e^{\lambda_i t_0} \quad , \tag{2.48}$$

$$\eta_0 = \sum_{i=1}^{4} \alpha_i A_i e^{\lambda_i t_0} \quad , \tag{2.49}$$

$$\dot{\eta}_0 = \sum_{i=1}^{4} \alpha_i \lambda_i A_i e^{\lambda_i t_0} \quad . \tag{2.50}$$

Selecting initial conditions such that $A_1 = A_2 = 0$, particular solutions containing only sine and cosine functions of the time for ξ and η are obtained,

$$\xi = \xi_0 \cos \omega_{xy} t + \frac{\eta_0}{\beta_3} \sin \omega_{xy} t \quad , \tag{2.51}$$

$$\eta = \eta_0 \cos \omega_{xy} t + \frac{\xi_0}{\beta_3} \sin \omega_{xy} t \quad , \tag{2.52}$$

where $\beta_3 = \dfrac{\omega_{xy}^2 - \Omega_{xx}^0}{2\omega_{xy}}$.

On the other hand, the general solution for ζ can be written in the following form,

$$\zeta = \zeta_0 \cos \omega_z t - \frac{\zeta_0}{\omega_z} \sin \omega_z t \tag{2.51}$$

From the linear approximation, the three-dimensional motion of spacecraft is not periodic since the in-plane and out-of-plane frequencies are not commensurate. However, ω_{xy} and ω_z are relatively close in value for the problem of interest. This suggests that quasi-periodic motion can be approximated.

2.6 Periodic Orbits in the vicinity of the Libration Points

There exist periodic orbits near the libration points in the two- and three-dimensional space [33-37] called Lyapunov and Halo orbits, respectively, whose sizes depend on the value of the Jacobi constant (see Fig. 2.2). If a spaceport is built on a Halo orbit about the L2 point, it is not hidden in the shadow of the secondary body

because the radius of the Halo orbits can be made larger than that of the secondary body. Thus, we will only consider the Halo orbit transfer case.

The computation of periodic orbits is generally time consuming unless a good initial guess is already available. Thus, development of a numerical method to improve an initial guess by predicting behavior near the reference solution is desirable. Such a method requires the information concerning the sensitivity of the state from changes in the initial guess. To gain insight into the sensitivities, it is useful to examine the evolution of a state vector by the state transition matrix in the vicinity of a reference solution. If a periodic orbit exists, it is possible to linearize about the periodic orbit. Equations (2.22)-(2.24) can be rewritten as six first-order differential equations where a state vector is defined as $\vec{q} = [x \quad y \quad z \quad \dot{x} \quad \dot{y} \quad \dot{z}]^T$.

$$\dot{\vec{q}} = f(\vec{q}) \quad . \tag{2.52}$$

Given some reference solution, $\vec{q}_{ref}$, to the differential equations, an approximation for the variations relative to the reference solution can be derived through a first-order Taylor series expansion about the reference. Ignoring the high order terms, the resulting linearized state variational equations are written as

$$\delta\dot{\vec{q}}(t) = A(t)\delta\vec{q}(t) \quad , \tag{2.53}$$

where $A(t) = \left.\frac{\partial f}{\partial \vec{q}}\right|_{\vec{q}_{ref}}$ is a 6 ×6, generally time-varying, matrix. It can be written in term of the following four 3 ×3 sub matrices,

$$A(t) = \begin{bmatrix} 0 & I_3 \\ \Omega_{ij} & C \end{bmatrix}, \tag{2.54}$$

where $\boldsymbol{0}$ represents the zero matrix and I_3 is the identity matrix. The C is defined as constant,

$$C = \begin{bmatrix} 0 & 2 & 0 \\ -2 & 0 & 0 \\ 0 & 0 & 0 \end{bmatrix}, \tag{2.55}$$

and Ω_{ij} has the form,

$$\Omega_{ij} = \begin{bmatrix} \Omega_{xx} & \Omega_{xy} & \Omega_{xz} \\ \Omega_{yx} & \Omega_{yy} & \Omega_{yz} \\ \Omega_{zx} & \Omega_{zy} & \Omega_{zz} \end{bmatrix}, \tag{2.56}$$

where the subscripts indicate second partial derivatives of the pseudo-potential evaluated on the reference solution. The solution to the linearized Equation (2.53) is

$$\delta\tilde{q}(t) = \Phi(t, t_0)\delta\tilde{q}(t_0) \tag{2.57}$$

where $\Phi(t, t_0)$ is the state transition matrix (STM). The expression in Eq. (2.57) relates variations in the trajectory at time t to the initial perturbation at time t_0. The STM is also described as a sensitivity matrix since it offers a linear prediction of the sensitivity of the trajectory to initial variations. Next, we consider the Poincaré section, Σ, which is transverse to the flow in three-dimensional space and reduces the dimension of the phase space by one (see Fig. 2.3). From some set of initial conditions in the Poincaré section, we propagate the equation of motions. At the time that the path crosses this section again, an intersecting point marks on this section. This point reflects a second crossing of the section. Thus, the point in the section is denoted a return map (Poincaré map). Therefore, the periodic orbit would be represented in this section by a single point, denoted as a fixed point, $\vec{q}^{\,*}$ (the periodic orbit intersects the same location in the section on every pass). Supposing the crossing period T, from Eq. (2.57),

$$\delta\tilde{q}(t_0 + T) = \Phi(t_0 + T, t_0)\delta\tilde{q}(t_0) \tag{2.58}$$

where $\Phi(t_0 + T, t_0)$ is called the Monodromy matrix. This Monodromy matrix is a linear stroboscopic map for the fixed point in the vicinity of the reference trajectory.

In this study, we compute the Halo orbits as follows. First, we assume the initial condition is $\vec{q}(t_0) = (x_0, 0, z_0, 0, \dot{y}_0, 0)$. Using the Runge-Kutta-Fehlberg method, the equations of motion are integrated keeping an allowance error below fourteenth-order until the sign of y changes twice, and the time at this point

is defined to be *t*. If $\vec{q}(t_0 + t) = (x_0, 0, z_0, 0, \dot{y}_0, 0)$, that orbit is considered to be a Halo orbit (*t* is considered to be a period of the Halo orbit, *T*, at this time). If the orbit does not close on itself at *t*, we use the state transition matrix to drive the norm of the difference $\vec{q}(t_0 + t) - \vec{q}(t_0)$ to a desired tolerance.

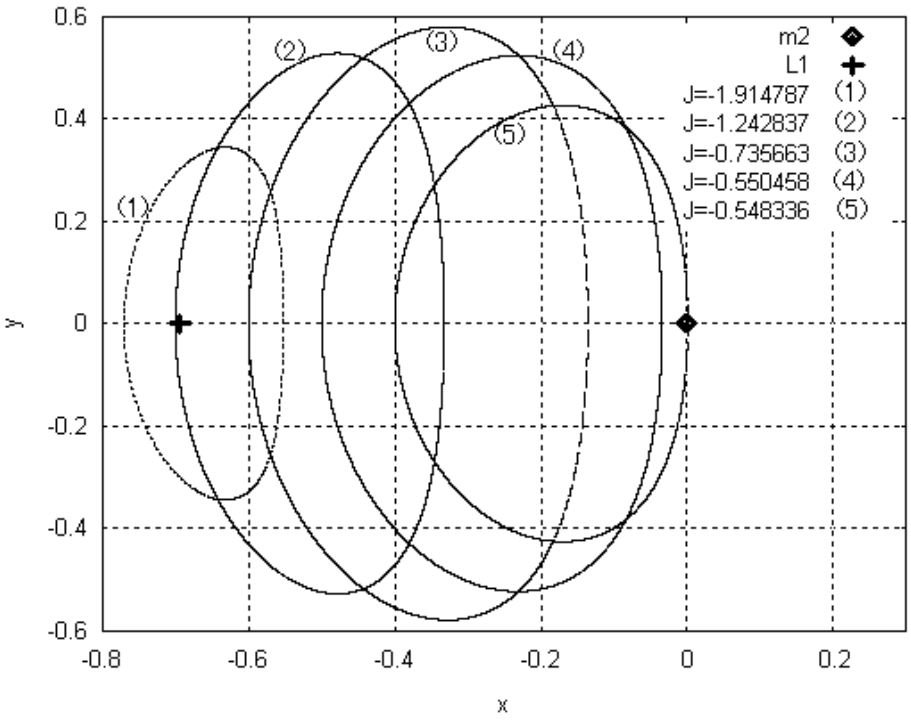

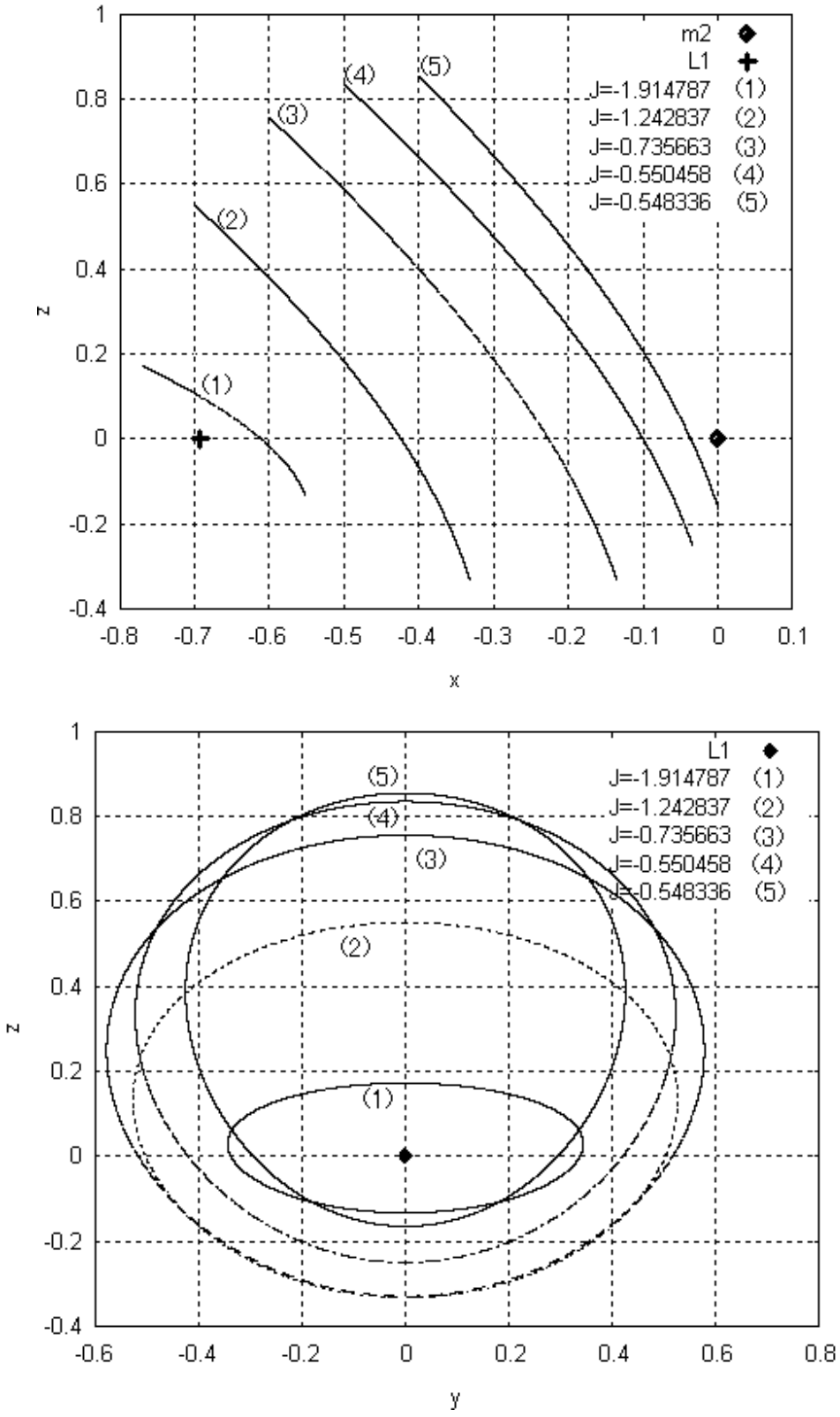

Figure 2.2: A few Halo orbits around L1.

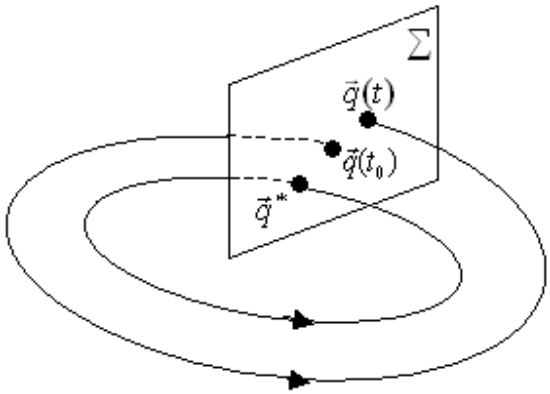

Figure 2.3: Periodic orbit and Poincaré section.

2.7 Invariant Manifold

There exist invariant structures associated with these periodic orbits, called unstable and stable manifolds [38, 39, 43]. These are trajectories that depart from or wind onto the periodic orbit with a nearly zero velocity correction, depending on whether they are stable or unstable, respectively. We exploit the unstable manifolds for escape trajectories from Halo orbit and the stable manifolds for capture trajectories to Halo orbits (see Fig. 2.4).

To obtain the manifolds, stability information associated with the periodic orbit, contained within the Monodromy matrix, is examined. According to Floquet theory [44], the STM can be rewritten as,

$$\Phi(t,t_0) = F(t)e^{Bt}F^{-1}(t_0) \quad , \tag{2.59}$$

where $F(t_0)$ is a periodic matrix and B is a constant diagonal matrix. After one period, where $t = t_0 + T$, $F(t_0+T) = F(t_0)$, Eq. (2.59) can be rewritten as,

$$e^{B(t_0+T)} = F^{-1}(t_0)\Phi(t_0+T,t_0)F(t_0) \quad . \tag{2.60}$$

Therefore, $F(t_0)$ and B contain the eigenvectors, $\vec{v}_i$, and the eigenvalues, λ_i, of the Monodromy matrix. The eigenvalues of the Monodromy matrix offer information about the phase space in the vicinity of the periodic

orbit because λ_i reflect the linear stability of the fixed point in the map. According to Lyapunov's Theorem, since the determinant of the Monodromy matrix is equal to one, the eigenvalues of the Monodromy matrix must occur in reciprocal pairs. Furthermore, one pair of eigenvalues must be equal to one at least because the orbit is periodic and any complex eigenvalue must be paired with its conjugate. For periodic orbits in the CR3BP, $\lambda_1 = \lambda_2 = 1$, λ_3 and λ_4 are complex conjugate eigenvalues located on the unit circle, and λ_5 and λ_6 are real with $\lambda_5 = \lambda_6^{-1}$. The flow in the region of phase space near a periodic orbit can be decomposed into three subspaces: the stable, unstable and center subspaces (E^s, E^u, E^c). Table 2.2 shows a relation between the subspace and the eigenvalues of the Monodromy matrix. Eigenvectors corresponding to a stable eigenvalue lie in the stable subspace and yield stable manifolds asymptotically approaching the periodic orbit as $t \to \infty$. Eigenvectors corresponding to an unstable eigenvalue lie in the unstable subspace and yield unstable manifolds asymptotically approaching the orbit as $t \to -\infty$. Eigenvectors corresponding to a center eigenvalue lie in the center subspace and yield trajectories neither approaching nor departing the periodic orbit as $t \to \pm\infty$. The directions defined by the eigenvectors associated with the stable/unstable subspace of the linear system are used to approximate the direction of the local stable and unstable manifolds. The local stable/unstable manifolds, W_l^s and W_l^u, are then propagated forward/backward in time to compute approximations to the global stable/unstable manifolds in the nonlinear system (W^s and W^u). At a fixed point, $\vec{q}^*$, corresponding stable and unstable eigenvectors, $\vec{v}^s(\vec{q}^*)$ and $\vec{v}^u(\vec{q}^*)$ are computed from the Monodromy matrix and normalized with respect to its position, these are,

$$\vec{v}_n^s = \frac{\vec{v}^s}{\sqrt{x_s^2 + y_s^2 + z_z^2}}, \tag{2.61}$$

$$\vec{v}_n^u = \frac{\vec{v}^u}{\sqrt{x_u^2 + y_u^2 + z_u^2}}. \tag{2.62}$$

The initial state vectors for the local stable and unstable manifolds are expressed as,

$$\vec{q}_0^s = \vec{q}^* \pm d\vec{v}_n^s \quad , \tag{2.63}$$

$$\vec{q}_0^{\,u} = \vec{q}^{\,*} \pm d\vec{v}_n^{\,u} \quad , \tag{2.64}$$

where d is the initial displacement from the periodic orbit. The initial displacement must be small enough to justify the linear approximation. A shift in the $+\vec{v}_n^{\,s}$ direction results in manifolds W_l^{s+} and W_l^{u+}, while the shift in the $-\vec{v}_n^{\,s}$ direction results in manifolds W_l^{s-} and W_l^{u-}. Thus, $\vec{q}_0^{\,s}$ and $\vec{q}_0^{\,u}$ are used to propagate forward/backward in time, and these propagation creates the global stable/unstable manifolds, W^{s+}, W^{s-}, W^{u+} and W^{u-} (see Fig. 2.5). Moreover, the global manifold is computed for each fixed point along the periodic orbit, the manifold surface is generated. In this paper, invariant global manifolds are generated by applying an infinitesimal impulse (the value of 0.00001 km/s in the Sun-Mars system) at each fixed point along the Halo orbit and integrated forward/backwards in time. The location on the periodic orbit is parameterized by a phase angle α on the periodic orbit (see Fig. 2.1).

Table 2.1: Relation between the subspace and the eigenvalue of the Monodromy matrix

Subspace	Eigenvalue of the Monodromy matrix
Unstable	$\lvert \lambda_i \rvert > 1$
Center	$\lvert \lambda_i \rvert = 1$
Stable	$\lvert \lambda_i \rvert < 1$

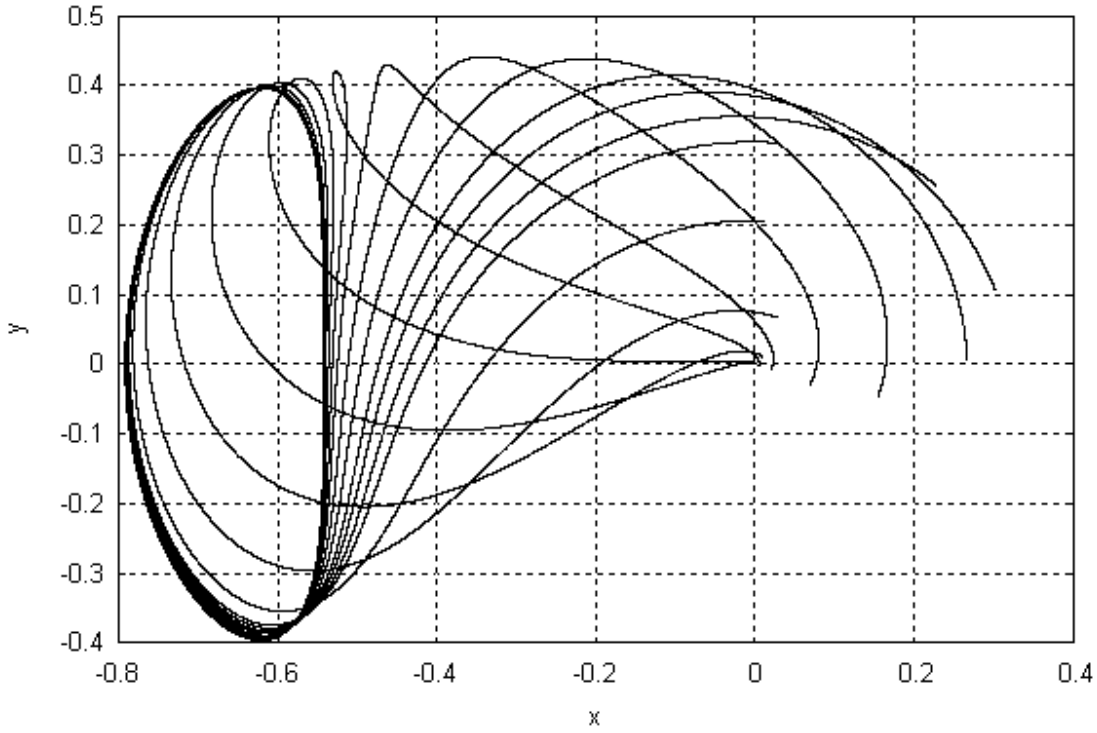

Figure 2.4: Stable manifold around L1 (represented until first Periapsis Point).

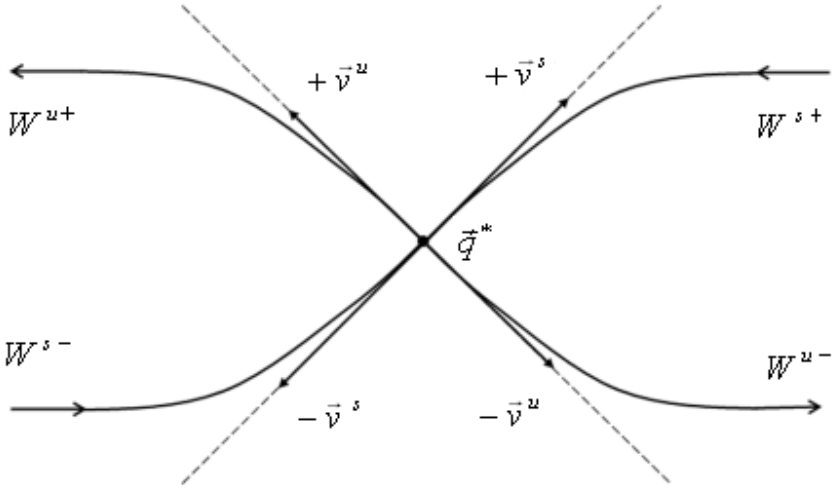

Figure 2.5: Stable and unstable manifolds tangent to eigenvectors.

CHAPTER 3

3 Escape and Capture Trajectories from and to Halo Orbits

3.1 Assumption of Escape Trajectories

In this study, we define that escape trajectories are trajectories that leave from a Halo orbit around Sun-Earth L1 or L2 using unstable manifolds and approach the Earth. Subsequently, at closest approach an impulsive maneuver is performed to escape from the Earth's gravitational dominance and put the spacecraft on an interplanetary trajectory (Fig. 3.1). The reason why an impulsive maneuver is performed near the surface of the Earth (perigee) is because it is the energetically efficient place to increase the escape energy. In this way, the unstable manifolds are used for escape trajectories from Halo orbits.

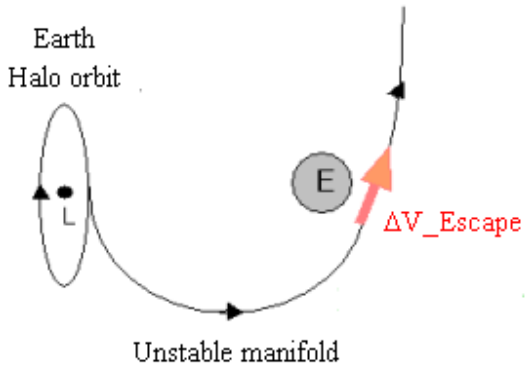

Figure 3.1: Example of escape impulsive trajectory from the Earth Halo orbit.

3.2 Assumption of Capture Trajectories

On the other hand, we assume that capture trajectories are trajectories that enter the sphere of influence of a target body from the interplanetary space and have a close flyby with the target body. At closest approach an impulsive maneuver is performed to put the spacecraft on a stable manifold that leads to capture to a Halo orbit around L1 or L2 of the target body (Fig. 3.2). The reason why an impulsive maneuver is performed near the surface of the target body (periapsis) is because this is the energetically efficient place to reduce the approach

energy, which may also be reduced by using an aero assist with the planetary atmosphere. Once placed on the stable manifold, the S/C approaches the Halo orbit, perhaps orbiting around the target body several times on its way. Once it is close to and crosses the Halo orbit a negligible impulsive maneuver is necessary to place it on the Halo orbit completely. In this way, the stable manifolds are used for capture trajectories to Halo orbits.

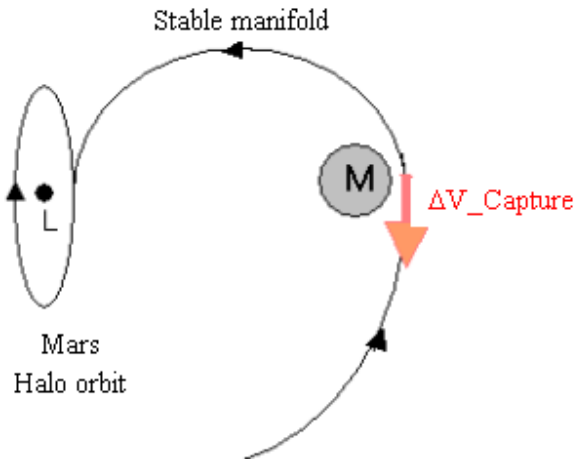

Figure 3.2: Example of capture impulsive trajectory to the Mars Halo orbit.

3.3 Characteristics of Periapsis Points of Invariant Manifolds

In this section, we investigate the first four periapsis passage points of invariant manifolds where an impulse maneuver may be performed for an interplanetary transfer. Unstable manifolds propagate forwards from a certain point on the Halo orbits in time. On the other hand, stable manifolds propagate backwards from a certain point on the Halo orbits in time.

3.3.1 Periapsis Location

Figure 3.3 shows an example of the first four periapsis passage points of one example trajectory of the L1 stable manifold (J = -2.01). The secondary body is located at the origin. Based on this result, Fig. 3.4 plots the first four periapsis point's locations of the L1 Halo stable manifold for several values of the Jacobi constant (i.e., the size of Halo orbits). The periapsis locations of stable and unstable manifolds of a L1/L2 Halo orbit are

symmetric to the *x-z* plane. Moreover, the periapsis locations of L1 unstable and L2 stable manifolds are symmetric to the *y-z* plane, and vice versa. We can see that each periapsis point region spreads out and that these periapsis locations depend on the value of the Jacobi constant.

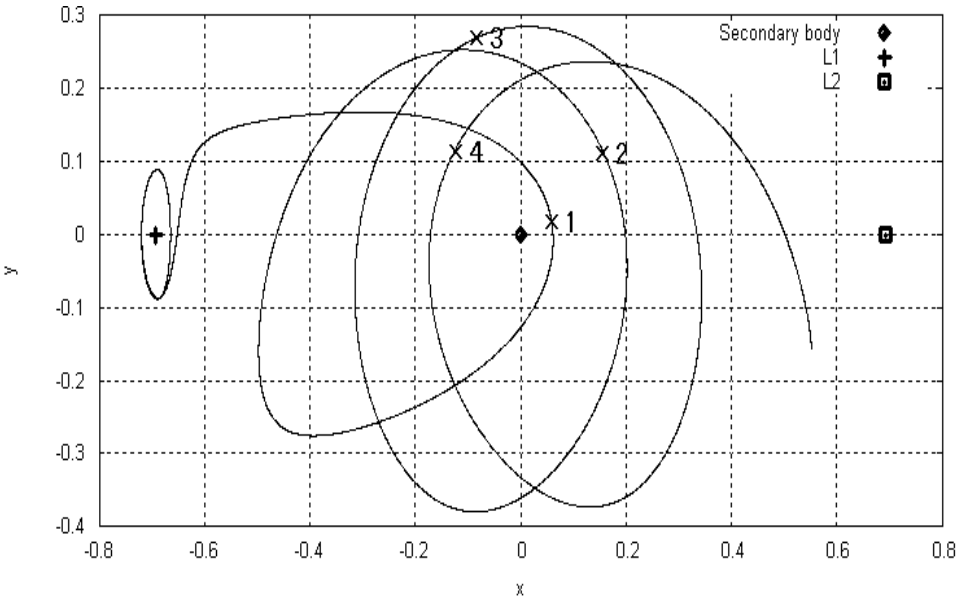

Figure 3.3: First four periapsis points of an example trajectory of the L1 stable manifold propagated backward from a certain point on the Halo orbit.

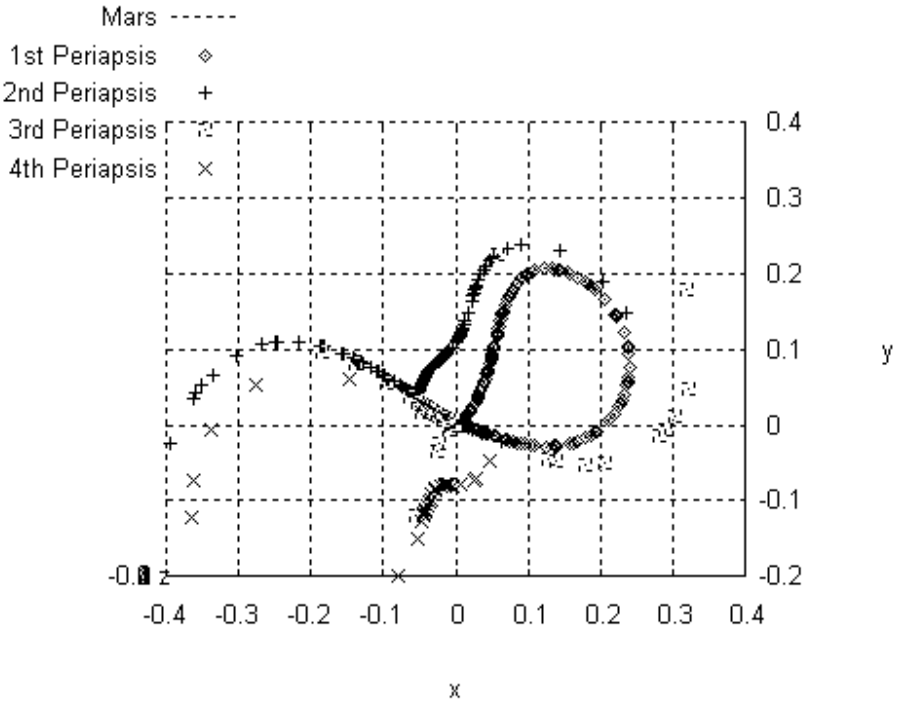
Mars
1st Periapsis
2nd Periapsis
3rd Periapsis
4th Periapsis
0.4
0.3
0.2
0.1
0
-0.1
-0.2
y
-0.4 -0.3 -0.2 -0.1 0 0.1 0.2 0.3 0.4
x

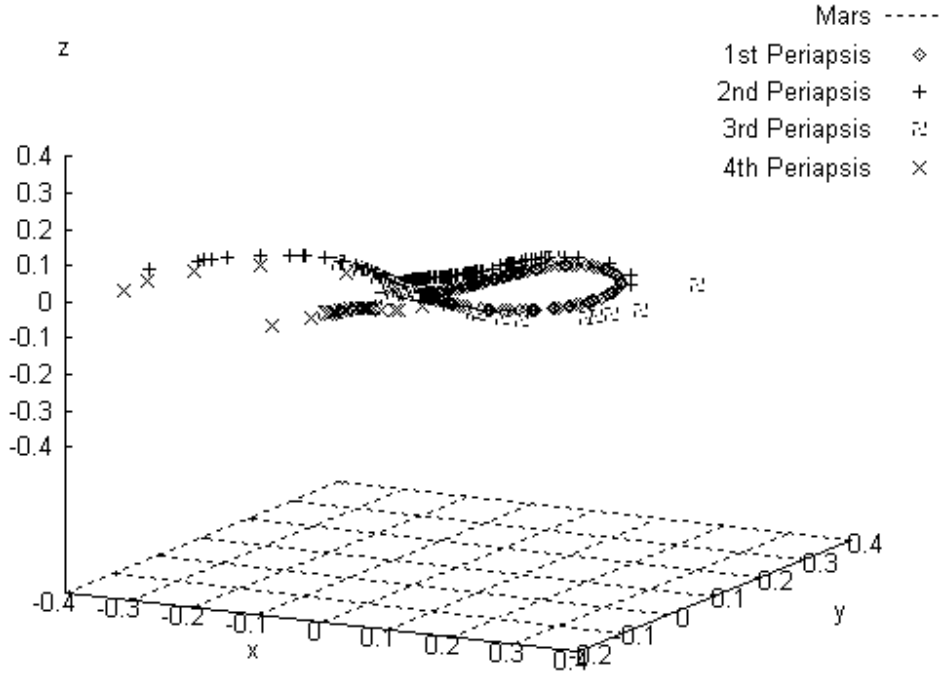
Mars
1st Periapsis
2nd Periapsis
3rd Periapsis
4th Periapsis
z
0.4
0.3
0.2
0.1
0
-0.1
-0.2
-0.3
-0.4
-0.4 -0.3 -0.2 -0.1 0 0.1 0.2 0.3 0.4
x
0.4 0.3 0.2 0.1 0 -0.1 -0.2
y

a) J = -2.01

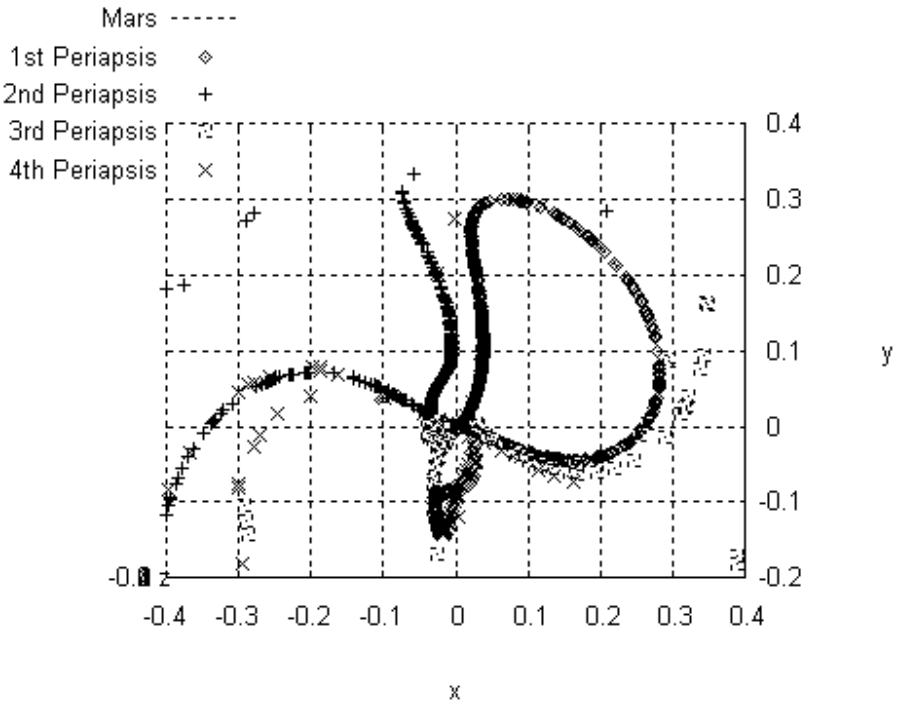
Mars
1st Periapsis
2nd Periapsis
3rd Periapsis
4th Periapsis
0.4
0.3
0.2
0.1
0
-0.1
-0.2
y
-0.4 -0.3 -0.2 -0.1 0 0.1 0.2 0.3 0.4
x

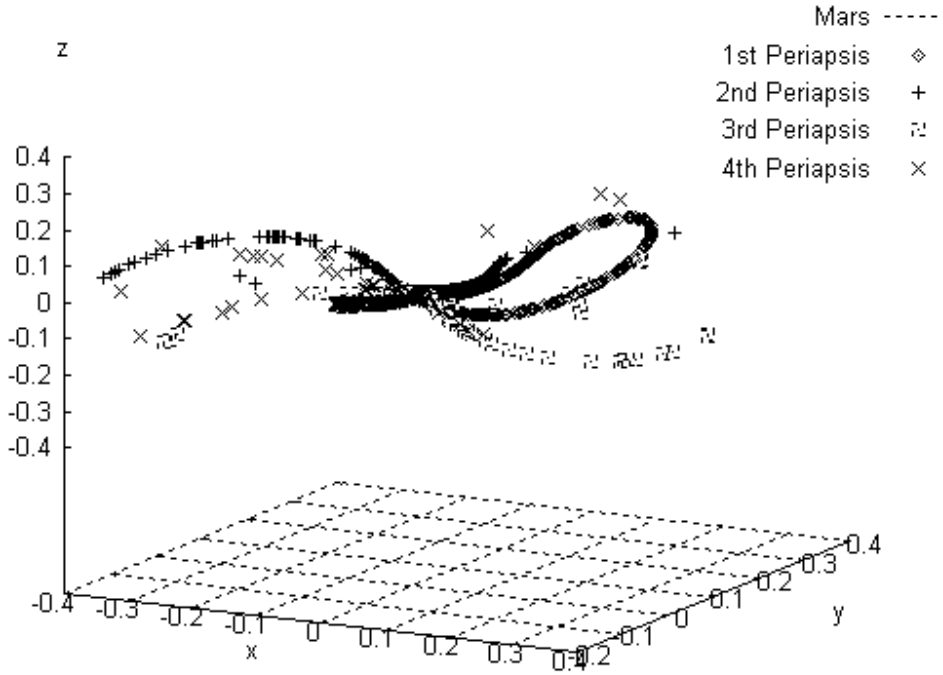
Mars
1st Periapsis
2nd Periapsis
3rd Periapsis
4th Periapsis
z
0.4
0.3
0.2
0.1
0
-0.1
-0.2
-0.3
-0.4
-0.4 -0.3 -0.2 -0.1 0 0.1 0.2 0.3 0.4
x
y

b) J = -1.84

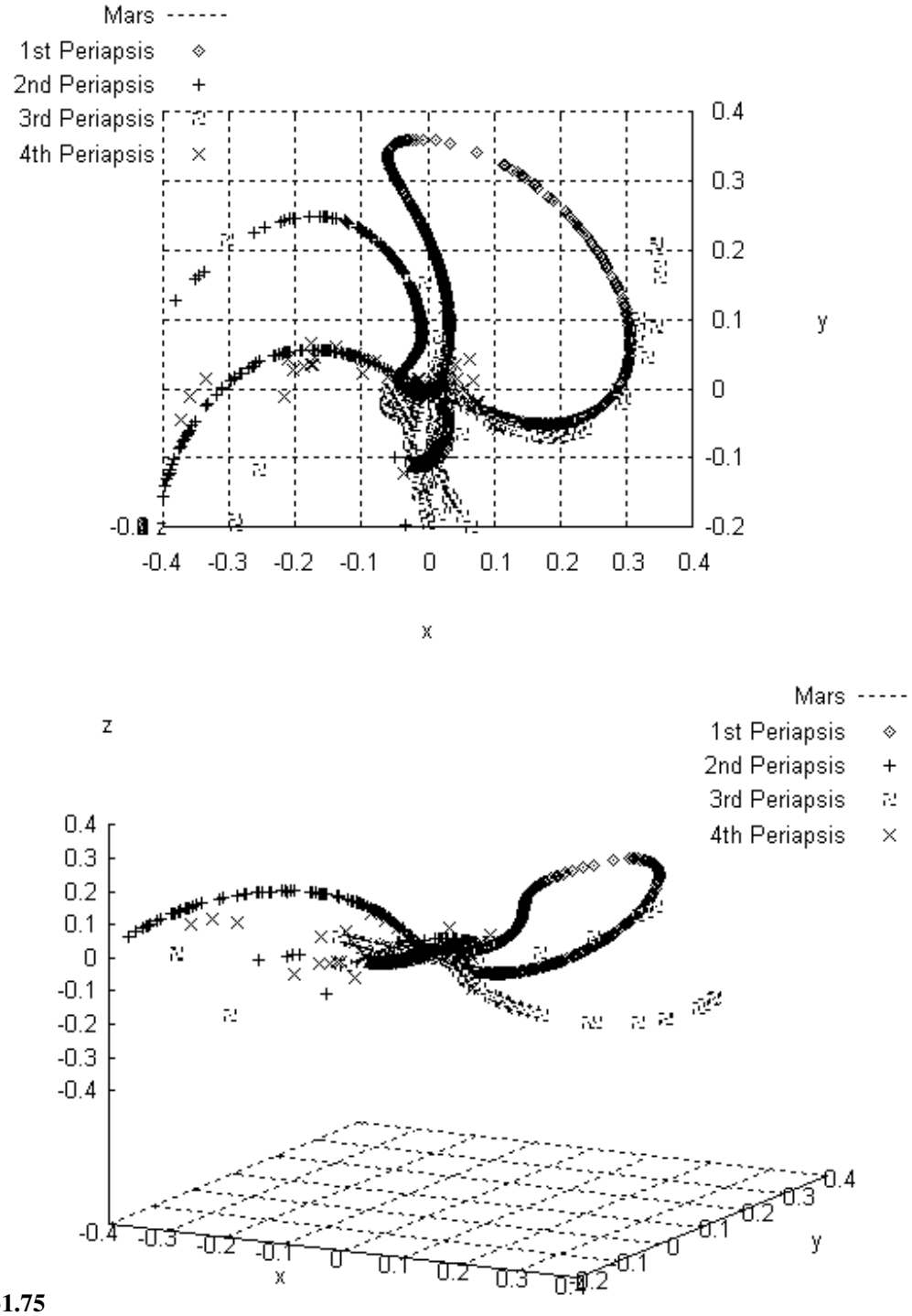

c) J = -1.75

Figure 3.4: First four periapsis locations of L1 Halo stable manifold. The secondary body is located at the origin.

3.3.2 Minimum Periapsis Distance

Figure 3.5 shows a relation between a minimum periapsis distance and the value of the Jacobi constant. The minimum periapsis distance means the distance from the origin to the periapsis point of stable manifold, which is closest to the origin in each of the four periapsis points in the same value of the Jacobi constant. The minimum periapsis distance decreases as the value of the Jacobi constant increases, and each four minimum periapsis distance becomes smaller than 0.000148 (which is smaller than the smallest normalized planetary radius, Neptune) when the value of the Jacobi constant is large. Thus the stable and unstable manifold of the first four periapsis passage points can intersect the surface of any of the planets in the solar system (but the size of the Halo orbit is limited). That is to say, a spacecraft can depart from the Halo orbit and approach the surface of the planet with the negligible velocity correction, and wind into the Halo orbit from the surface of the planet with negligible velocity correction by changing the size of the Halo orbit.

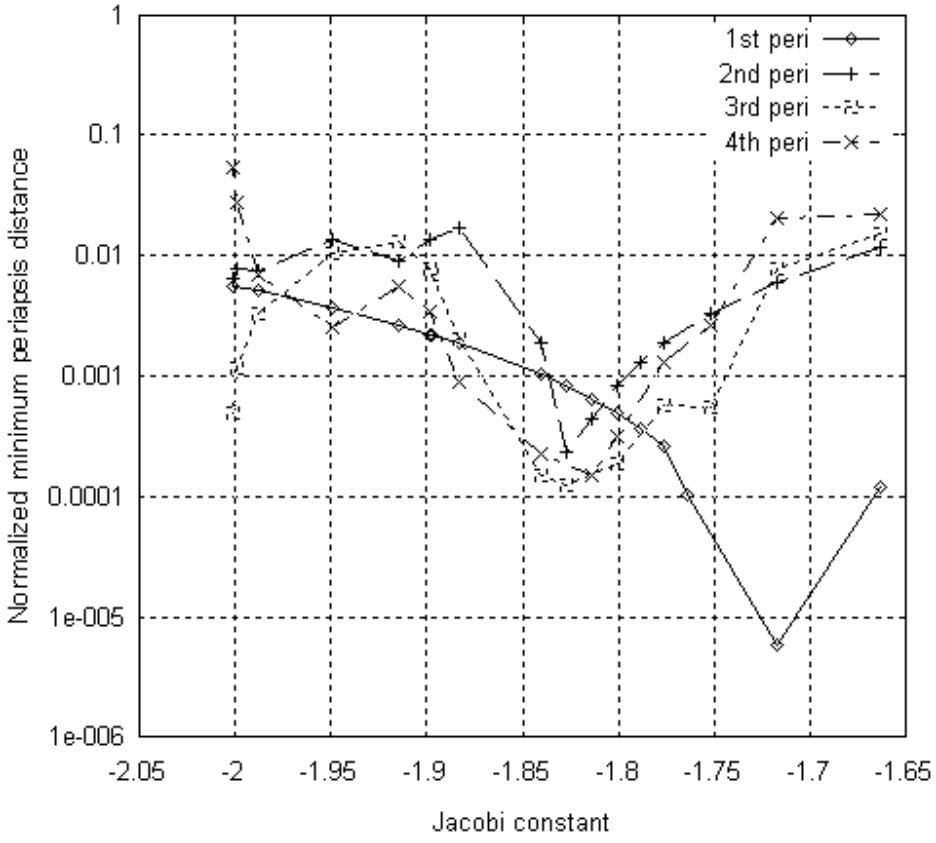

Figure 3.5: Minimum periapsis distance as a function of the value of the Jacobi constant.

3.3.3 Fast and Slow Transfer

In the same size of Halo orbits, there exist fast transfers and slow transfers which have same altitude of periapsis (P_f and P_s) as shown in Figs 3.6 and 3.7. These TOF from a Halo orbit to periapsis are different (e.g., fast transfer to P_f = 1.74 years, slow transfer to P_s = 1.86 years). They are obtained by different initial positions at a Halo orbit.

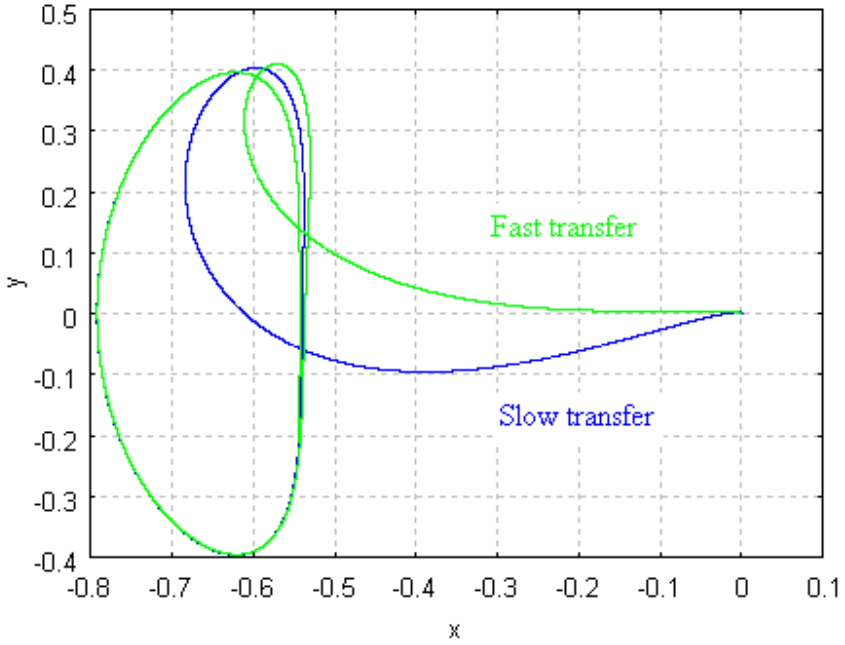

Figure 3.6: Fast and slow transfers between planet's periapsis and Halo orbit.

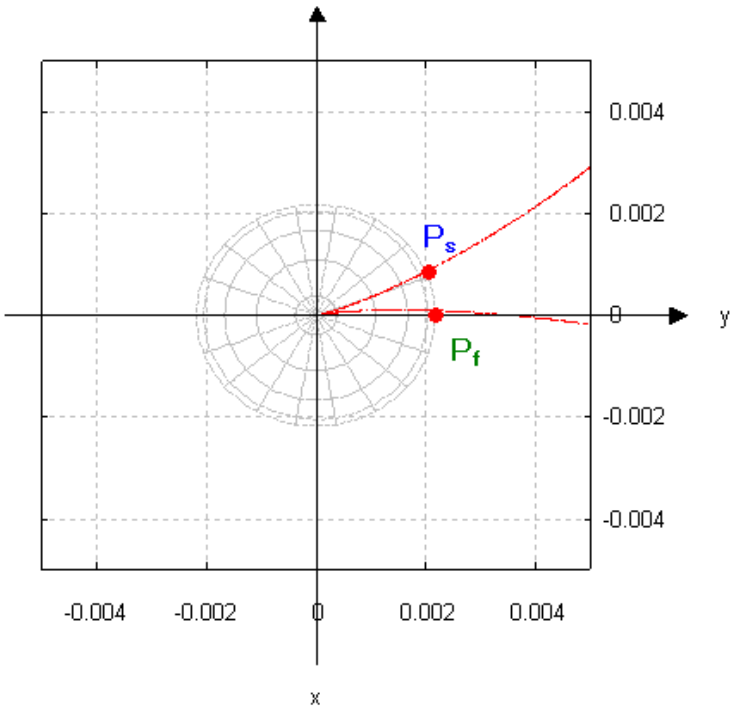

Figure 3.7: Periapsis of fast and slow manifold transfers.

3.3.4 Position and Velocity of Periapsis near the Surface of Planets

Next, Figs 3.8 – 3.13 show the position and the speed of the first periapsis of the Earth "L1" unstable manifolds near the Earth surface (altitude = 300 km) as a function of the Jacobi constant in the Sun-Earth fixed frame. The *x* and *y* components of position and velocity of Earth "L2" unstable manifolds is symmetric to that of Earth "L1" unstable manifolds. According to the Fig. 3.13, since the *z* direction component of velocity increases as the value of the Jacobi constant (the size of Halo orbits) increases, we should select small size Halo orbits. At this time, the *y* direction component of velocity is positive with the small value of the Jacobi constant form Fig. 3.12.

On the other hand, Figs 3.14 – 3.19 show the position and the velocity of the first periapsis of the Mars "L2" stable manifolds near the Mars surface (altitude = 200 km) as a function of the Jacobi constant in the Sun-Mars fixed frame. In the same way as the Earth unstable manifolds, we should select small Halo orbits since the *z* direction component of velocity increases as the value of the Jacobi constant increases as shown in Fig. 3.19. Moreover, the *y* direction component of velocity is negative with the small Halo orbit form Fig. 3.18.

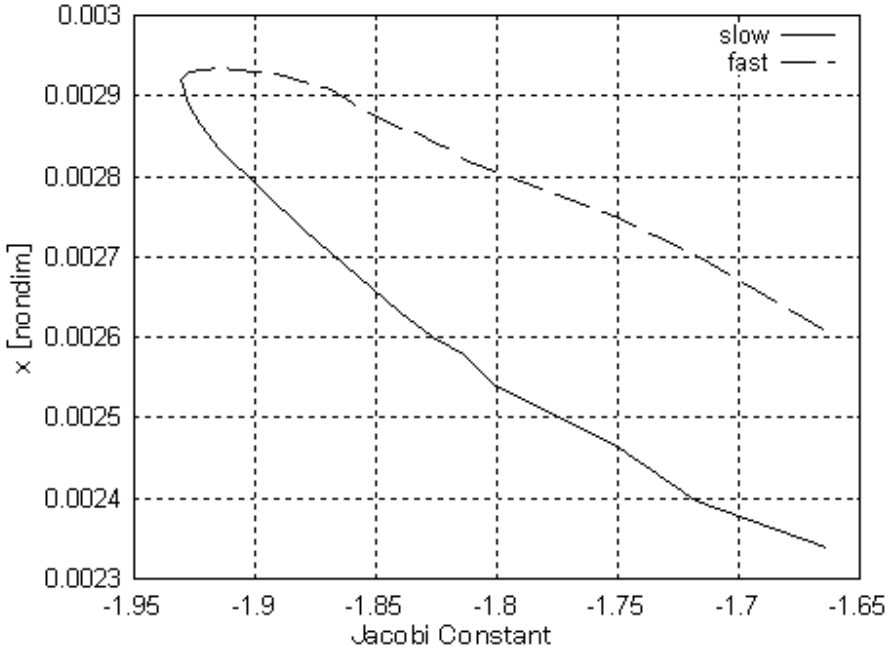

Figure 3.8: *x*-coordinate of periapsis of Earth L1 unstable manifolds as a function of the Jacobi constant.

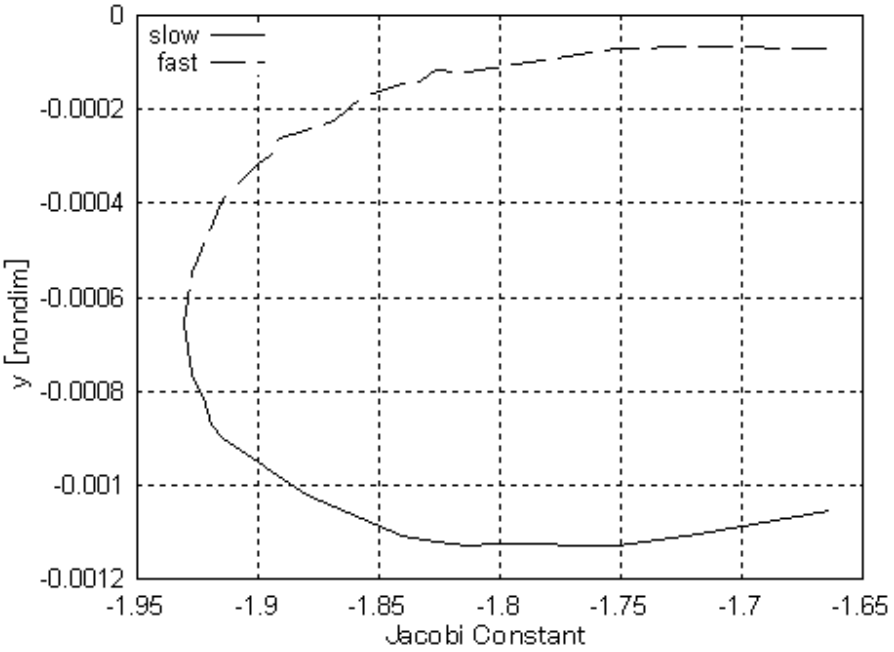

Figure 3.9: *y*-coordinate of periapsis of Earth L1 unstable manifolds as a function of the Jacobi constant.

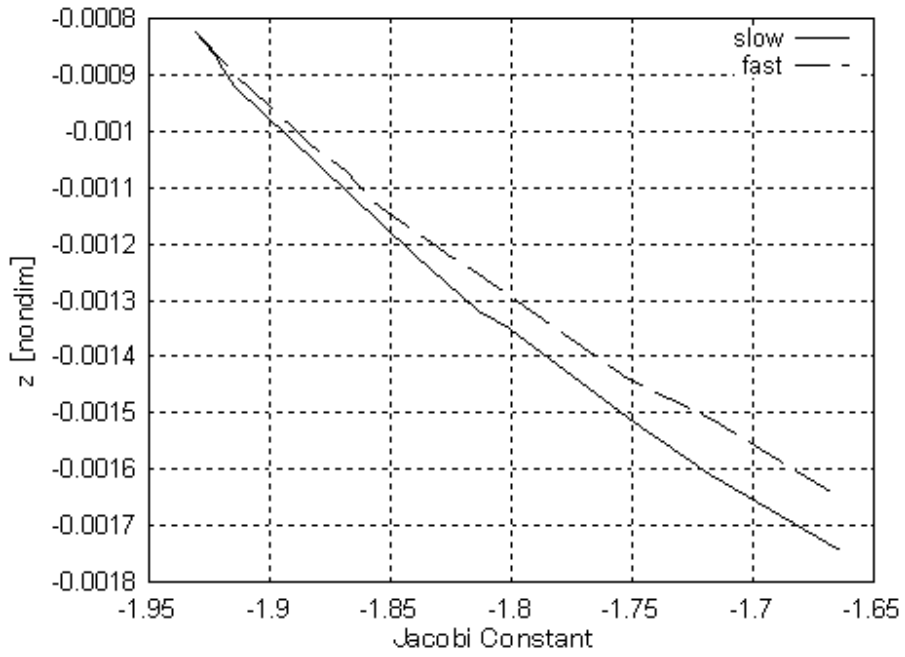

Figure 3.10: *z*-coordinate of periapsis of Earth L1 unstable manifolds as a function of Jacobi constant.

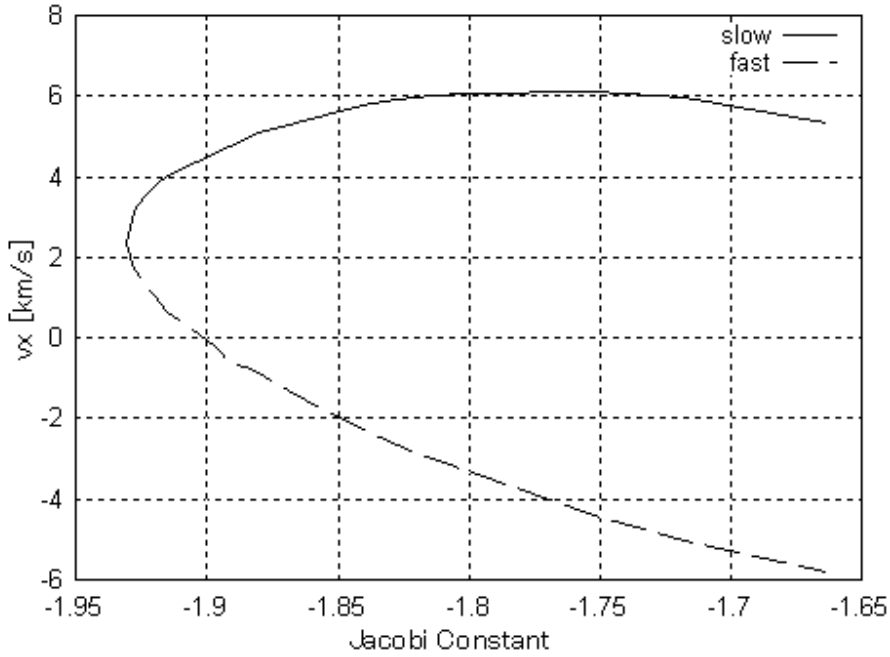

Figure 3.11: v_x component of periapsis velocity of Earth L1 unstable manifolds as a function of the Jacobi constant.

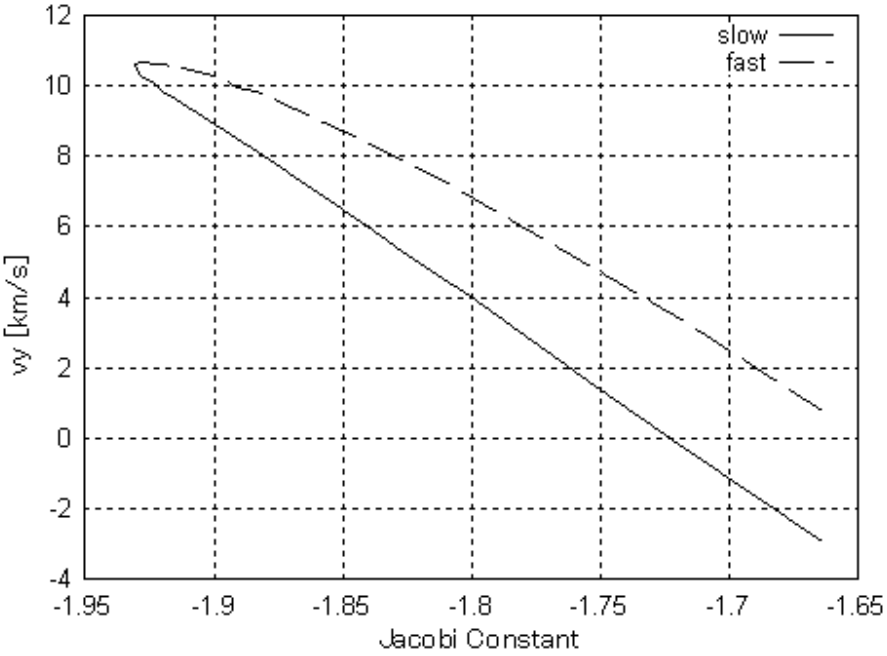

Figure 3.12: v_y component of periapsis velocity of Earth L1 unstable manifolds as a function of the Jacobi constant.

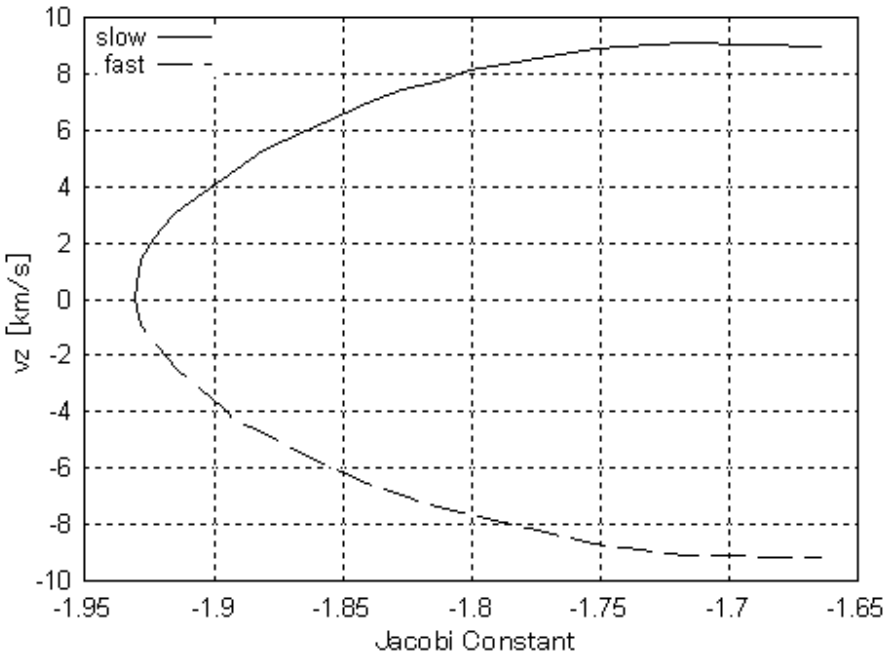

Figure 3.13: v_z component of periapsis velocity of Earth L1 unstable manifolds as a function of the Jacobi constant.

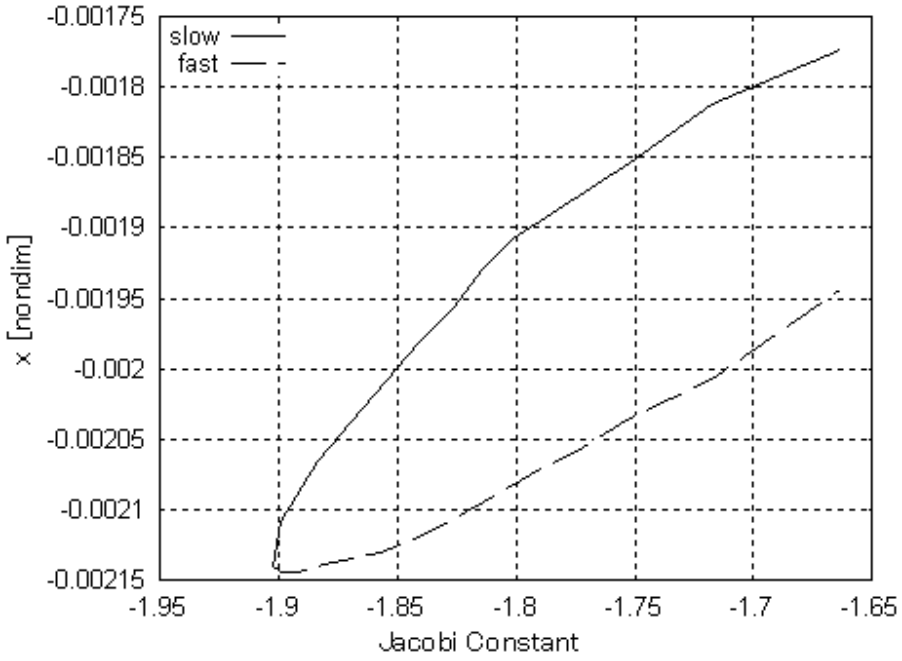

Figure 3.14: *x*-coordinate of periapsis of Mars L2 stable manifold as a function of the Jacobi constant.

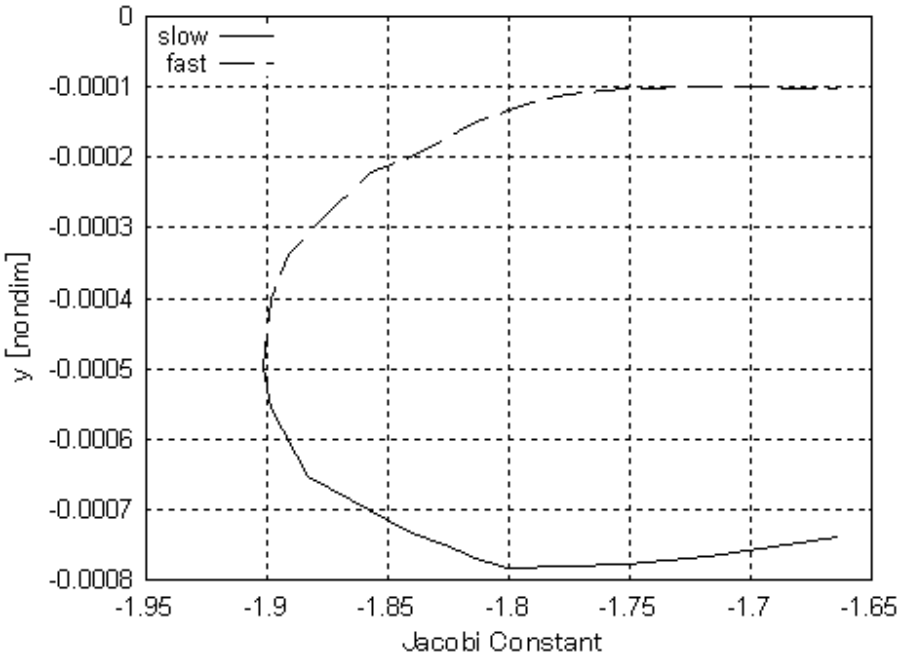

Figure 3.15: *y*-coordinate of periapsis of Mars L2 stable manifold as a function of the Jacobi constant.

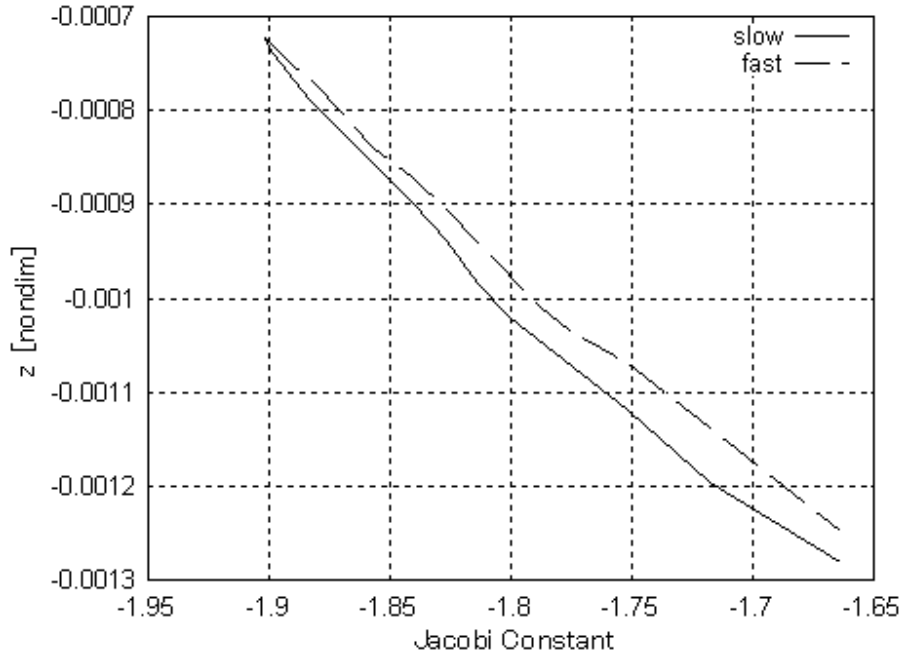

Figure 3.16: z-coordinate of periapsis of Mars L2 stable manifold as a function of the Jacobi constant.

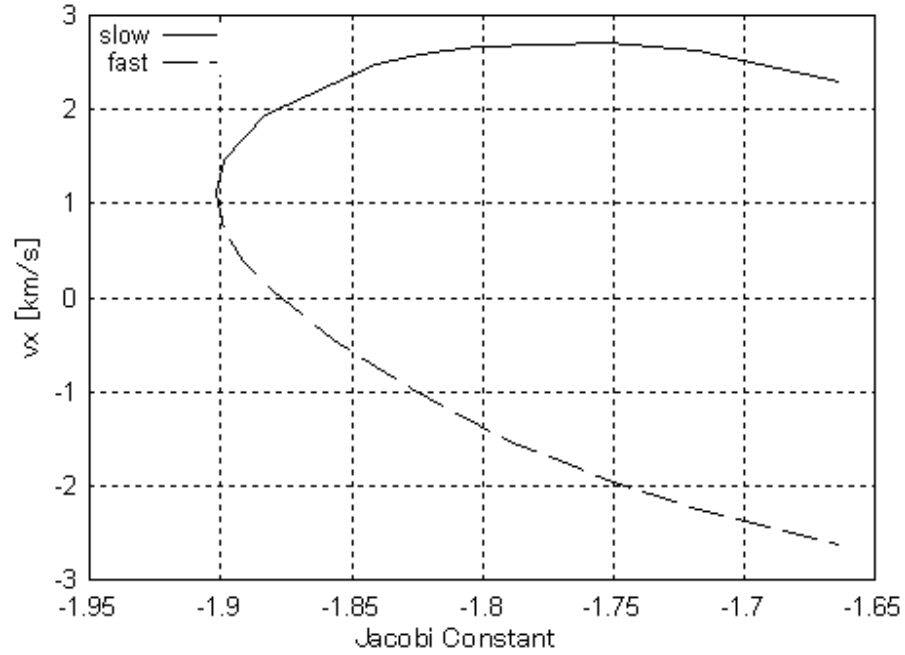

Figure 3.17: v_x component of periapsis velocity of Mars L2 stable manifold as a function of the Jacobi constant.

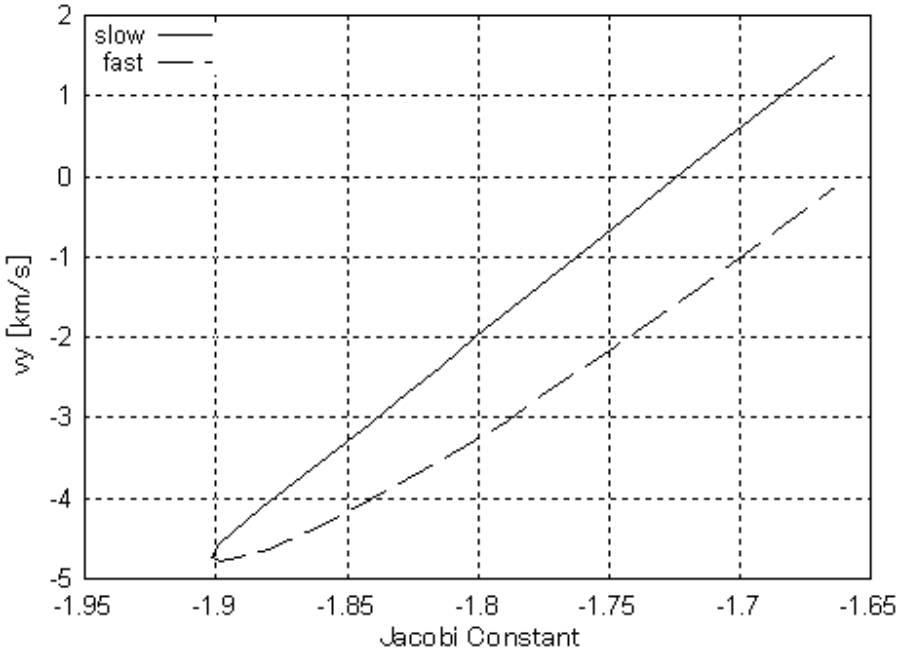

Figure 3.18: v_y component of periapsis velocity of Mars L2 stable manifold as a function of the Jacobi constant.

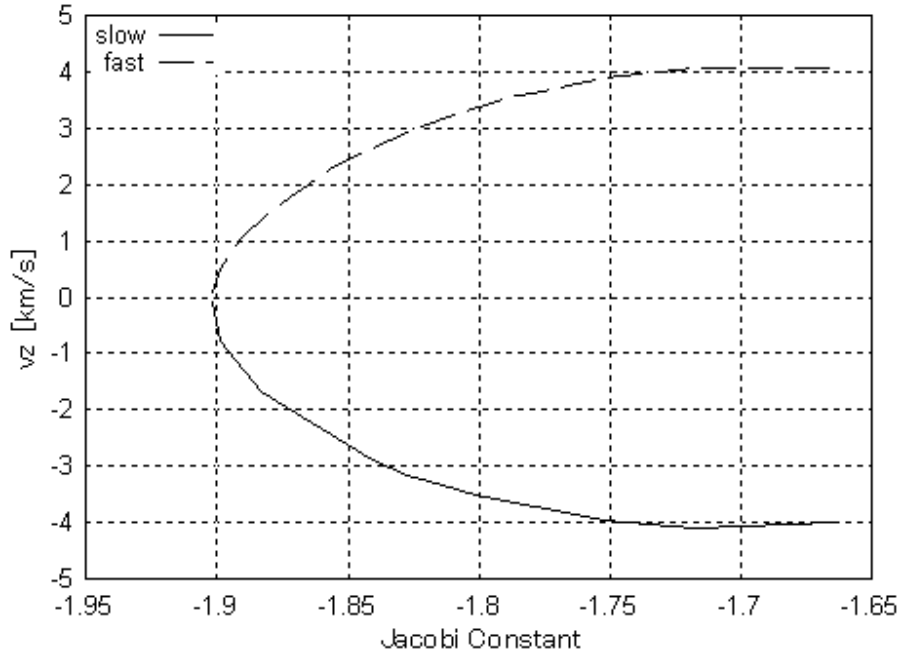

Figure 3.19: v_z component of periapsis velocity of Mars L2 stable manifold as a function of the Jacobi constant.

3.4 Comparison with Periapsis of Trajectories from/to L1 or L2 Points

By way of comparison, we consider a two-impulse transfer from the Sun-Earth L1/L2 point to the Earth (altitude = 300 km). In Fig. 3.20, there exist two classes of ballistic transfers; one is a fast transfer (ΔV is around 342 m/s at L1/L2 and the TOF is around 35 days), the other is a slow transfer (ΔV is around 279 m/s at L1/L2 and the TOF is around 117 days) [12]. On the other hand, the required ΔV at Halo orbit for the transfer from the Halo orbit to Earth is almost zero. Moreover, the magnitude of velocity at perigee from L1/L2 points is almost the same as that of the transfer from Earth Halo orbit. Therefore, it is better to put the spaceport on the Halo orbit of Earth and a target body than to put on L1/L2 point from the view of the ΔV.

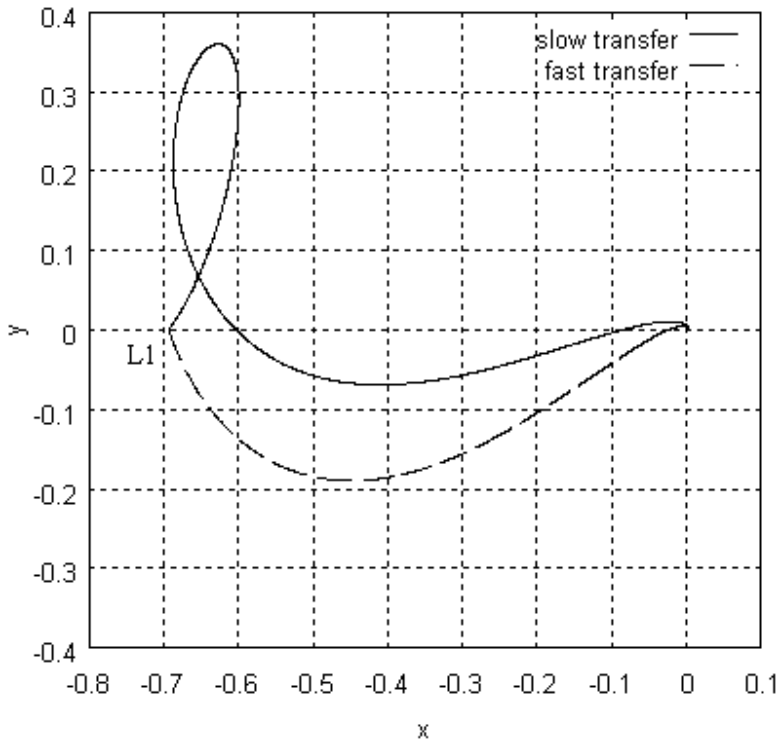

Figure 3.20: Transfer between L1 point and secondary body.

3.5 Summary

First, we defined the escape and capture trajectories from/to Halo orbit using the impulsive maneuver at the periapsis of manifold. And then, the characteristics of the periapsis of manifold, where an impulsive maneuver would be performed for the interplanetary transfer, were investigated. As a result, the stable and unstable manifolds could intersect the surface of any of the planets by changing the size of the Halo orbits. Namely, a spacecraft could leave the Halo orbit and come close to the surface of the planet with the negligible velocity correction, and wind into the Halo orbit from the surface of the planet with negligible velocity corrections. Moreover, the position and the velocity of the manifold at periapsis near the surface of planets are discussed.

CHAPTER 4

4 Reduction of the Time of Flight for Escape and Capture from/to Halo Orbit

In the previous chapter, the periapsis of stable and unstable manifolds associated with the Halo orbits are investigated. As a result, it was found that the impulsive maneuver could be performed at the surface of any of the planets in the solar system using the unstable and stable manifolds. However, the time of flight (TOF) is long for our escape and capture on the Halo orbit using the unstable and stable manifold because the manifolds generally orbit around the L1/L2 point several times. For instance, the TOF is approximately 1.9 years for the capture using stable manifold from Mars periapsis to the arrival point on the Halo orbit in Fig. 4.1, where the points in the figure are plotted every month. It is not feasible, thus a reduction of the TOF for the escape and the capture is discussed.

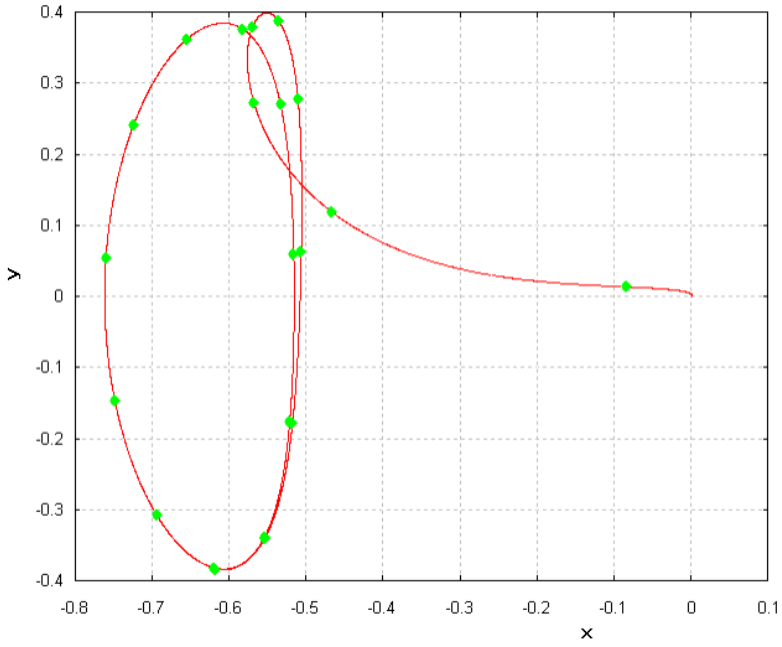

Figure 4.1: Example capture trajectory to Mars Halo orbit for J = -2.01

4.1 Time of Flight Reduction

We assume performing ΔV_{peri} and ΔV_{HO} at both the periapsis of manifold and the point on Halo orbit, respectively, to reduce TOF for escape and capture (two-impulse escape and capture as shown in Fig. 4.2). Here, we focus on the capture case, but a similar method can be followed for the escape case. As the total ΔV ($\Delta V_{peri} + \Delta V_{HO}$) increases, the shape of the capture trajectories varies as shown in Fig. 4.3 (the values are for the capture to Mars Halo orbit). As mentioned in chapter 3, there exist two families of the capture trajectories approaching Mars. We define the trajectory family as the slow captures (*S*), and the trajectory family as the fast captures (*F*). Figure 4.4 plots the TOF against the required total ΔV for the capture from Mars periapsis to the Halo orbits. Each parabola line means the relation between the TOF and the required total ΔV with respect to each arrival point where is performed ΔV_{HO}. The vertex of a parabola represents the minimum required ΔV with respect to the arrival point (Figure 4.5). In fact, depending on the applied direction, TOF not only increases but also decreases as the total ΔV to reach each arrival point in Fig. 4.6 increases. From this result, TOF could be reduced more than a year by performing a ΔV of only 0.06 km/s. It is a significant improvement by performing a decent ΔV. Moreover, it was found that TOF has a linear relation with the logarithm of the minimum required ΔV in the both slow and fast capture families. Even changing the size of Halo orbits, TOF also has a linear relation with the logarithm of the minimum required ΔV (see Fig. 4.7).

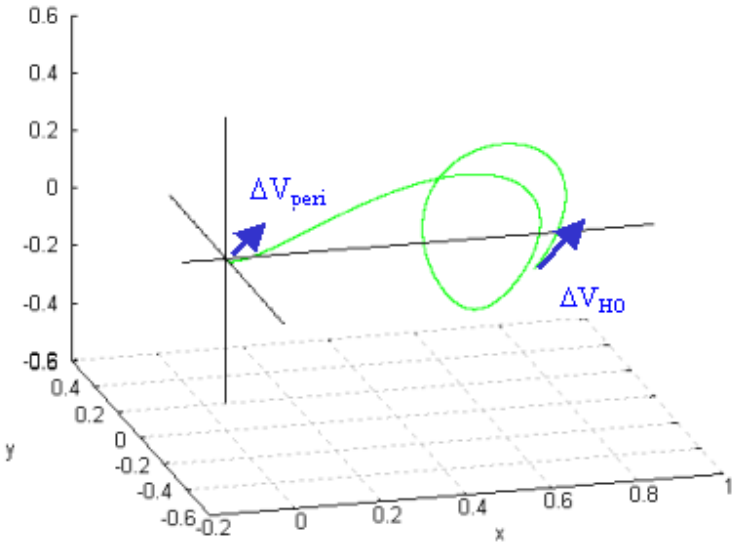

Figure 4.2: Two-impulse capture to reduce the TOF, also applicable to escape.

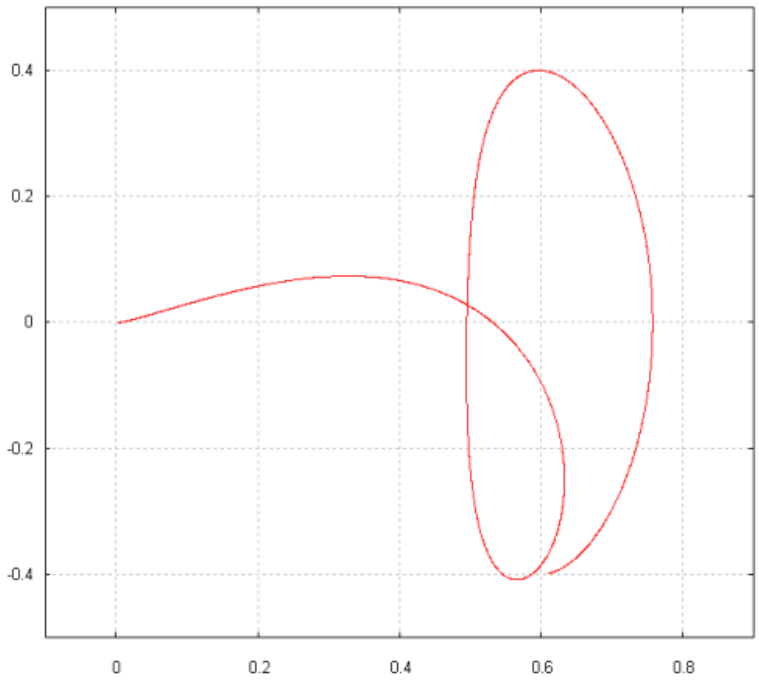

(*S*-1) ΔV = 2.22e-5 km/s & TOF = 1.28 years

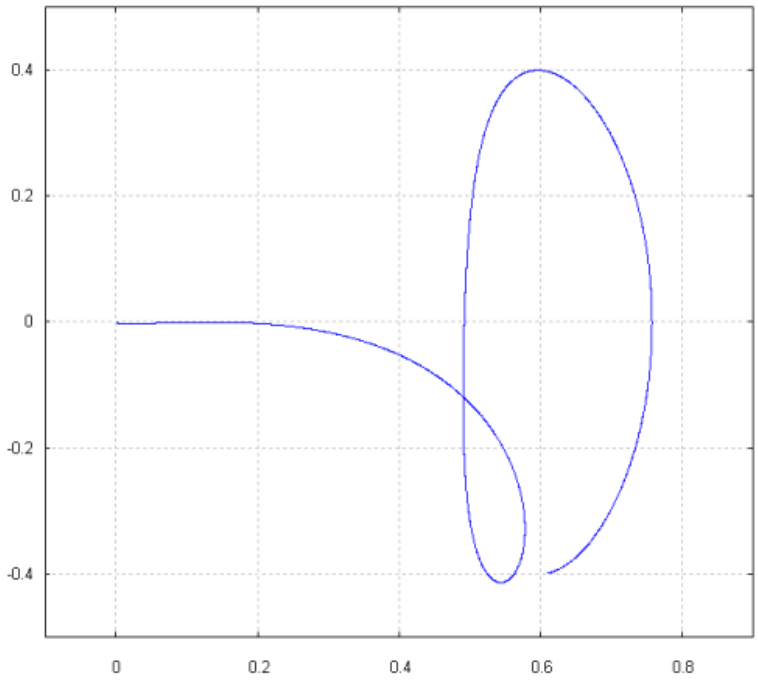

(*F*-1) ΔV = 4.08e-5 km/s & TOF = 1.21 years

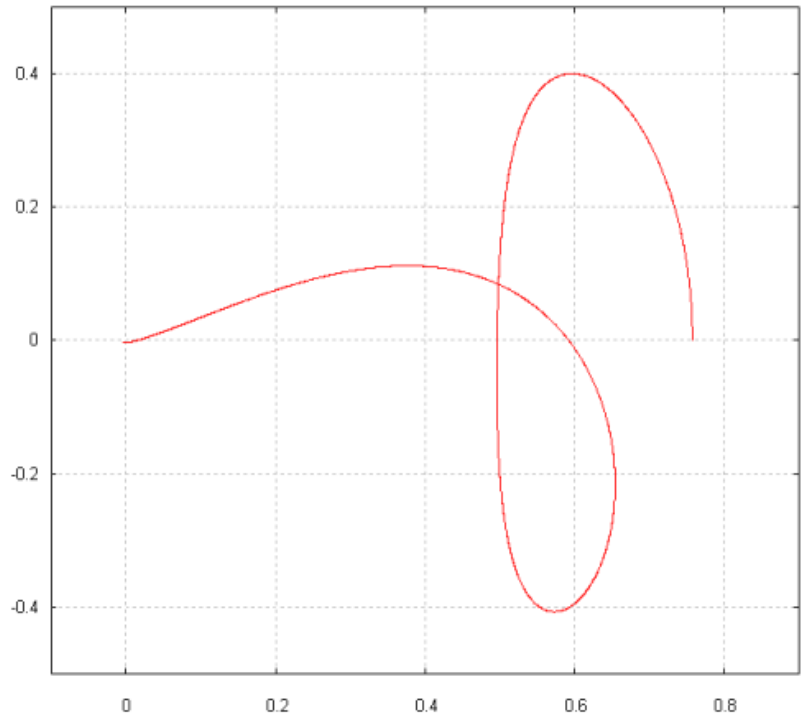

(*S*-2) ΔV = 1.28e-4 km/s & TOF = 1.05 years

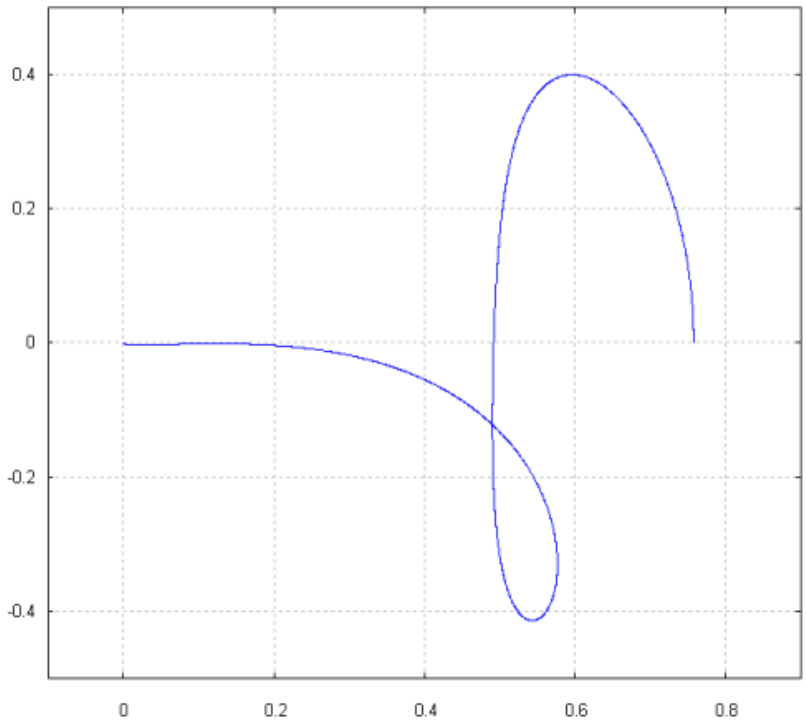

(*F*-2) ΔV = 2.34e-4 km/s & TOF = 0.98 years

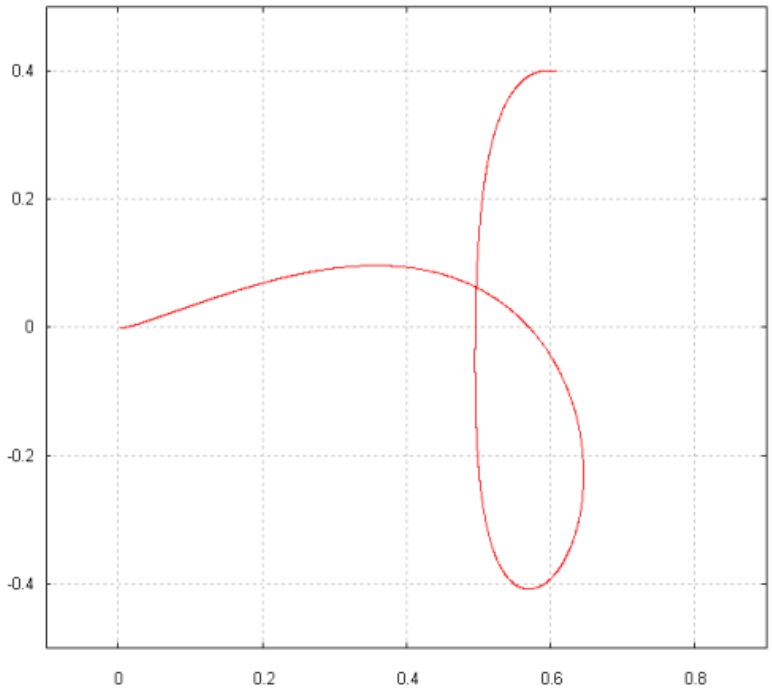

(*S*-3) ΔV = 6.37e-4 km/s & TOF = 0.82 years

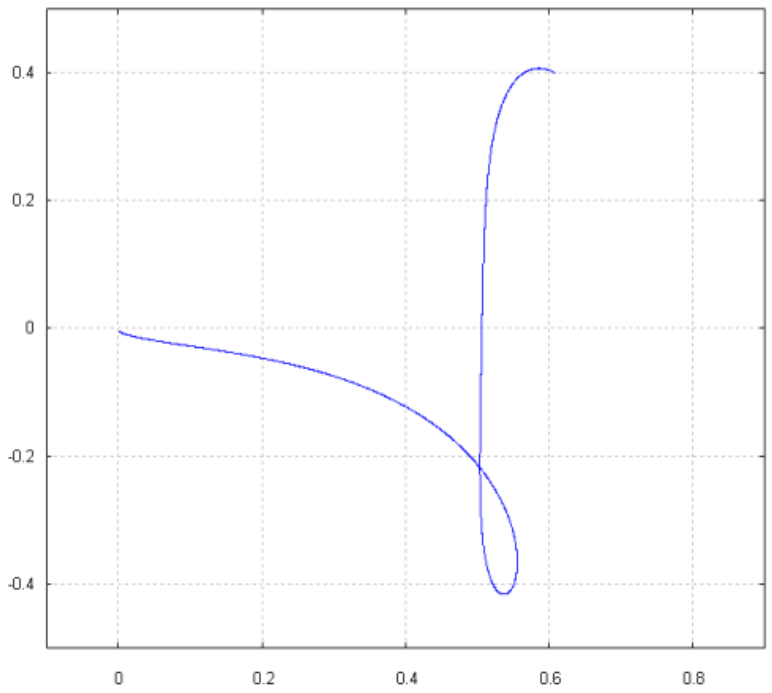

(*F*-3) ΔV = 1.18e-3 km/s & TOF = 0.75 years

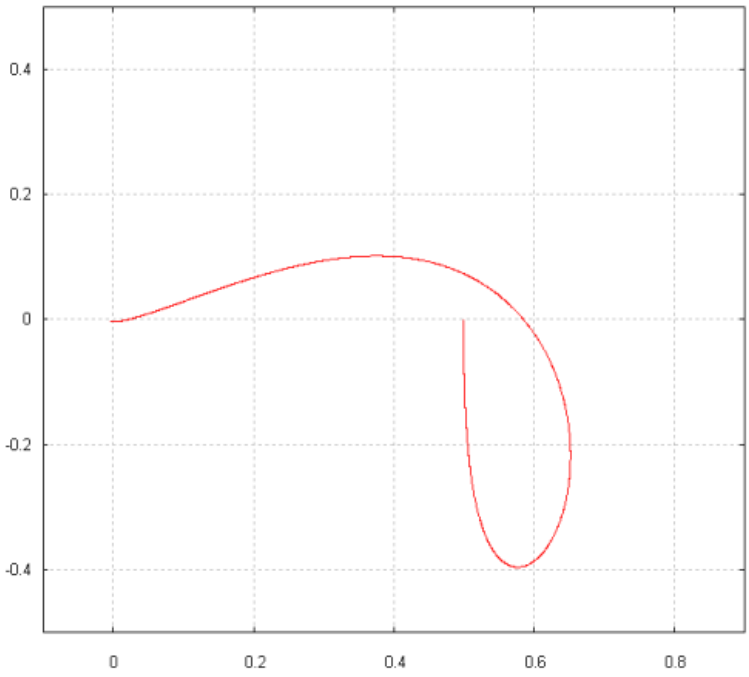

(*S*-4) ΔV = 3.43e-3 km/s & TOF = 0.59 years

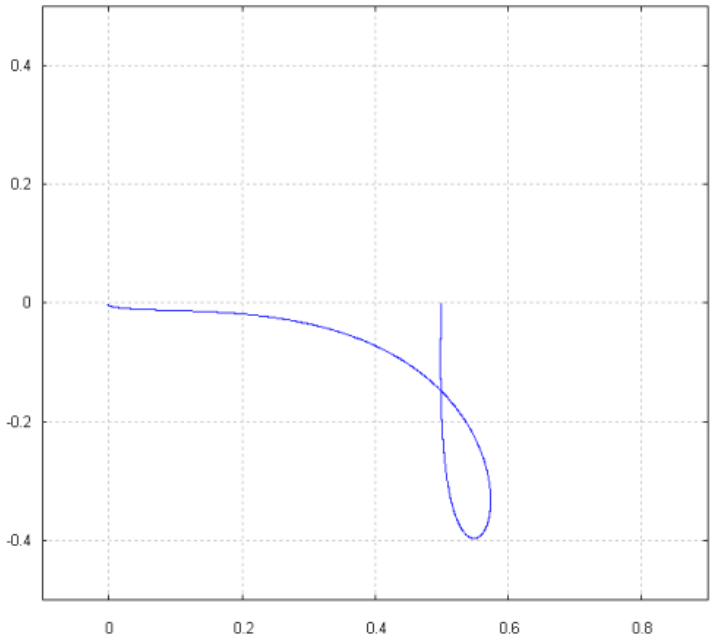

(*F*-4) ΔV = 5.87e-2 km/s & TOF = 0.53 years

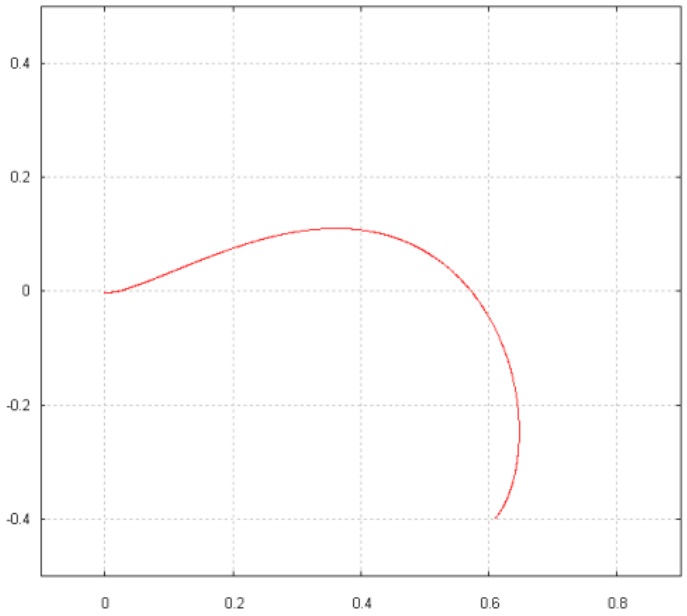

(*S*-5) ΔV = 2.44e-2 km/s & TOF = 0.36 years

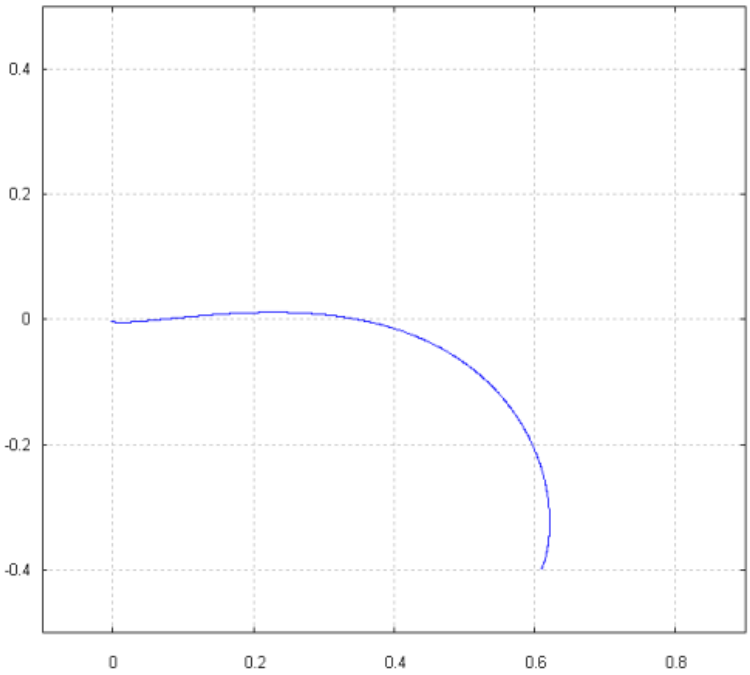

(*F*-5) ΔV = 3.79e-2 km/s & TOF = 0.32 years

Figure 4.3: Shape of the capture trajectories as increasing ΔV in the *x*-*y* plane.

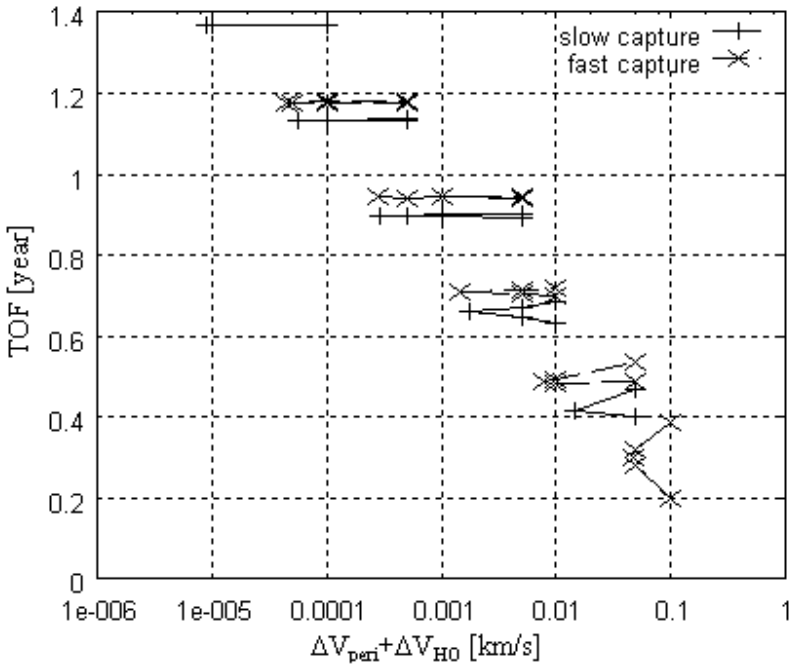

Figure 4.4: Relation between the TOF and ΔV (*J* = -1.85)

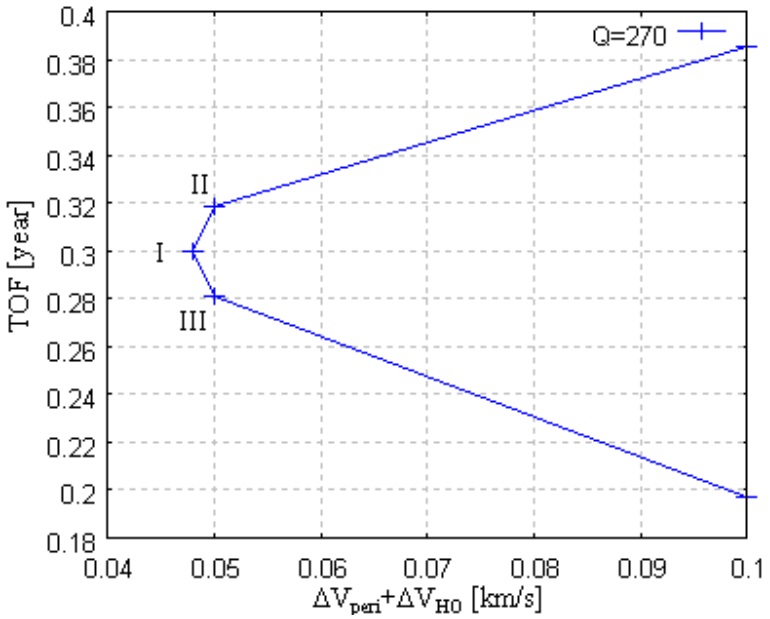

Figure 4.5: Minimum required ΔV for the capture to the arrival point

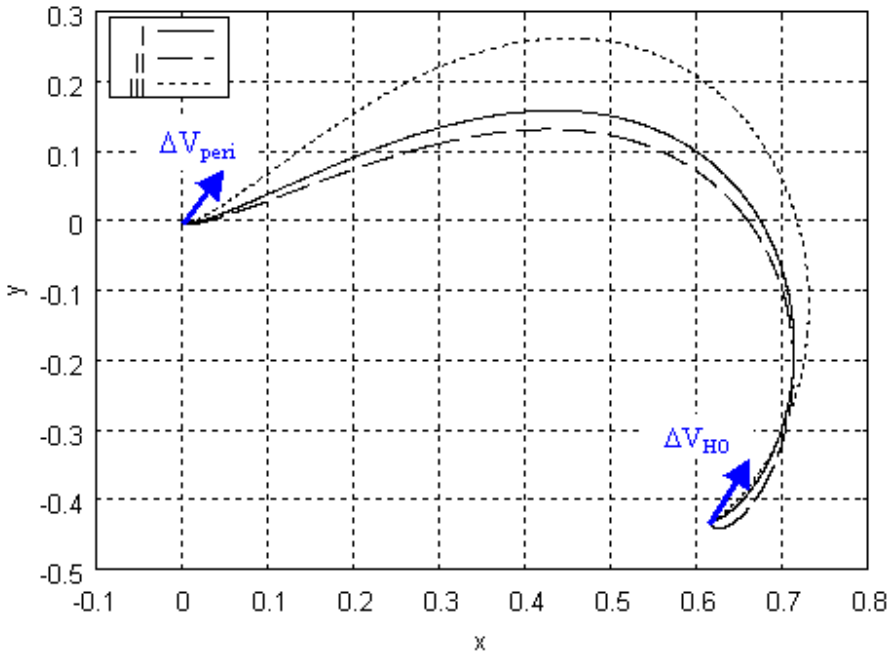

Figure 4.6: Capture trajectories of minimum required ΔV and others.

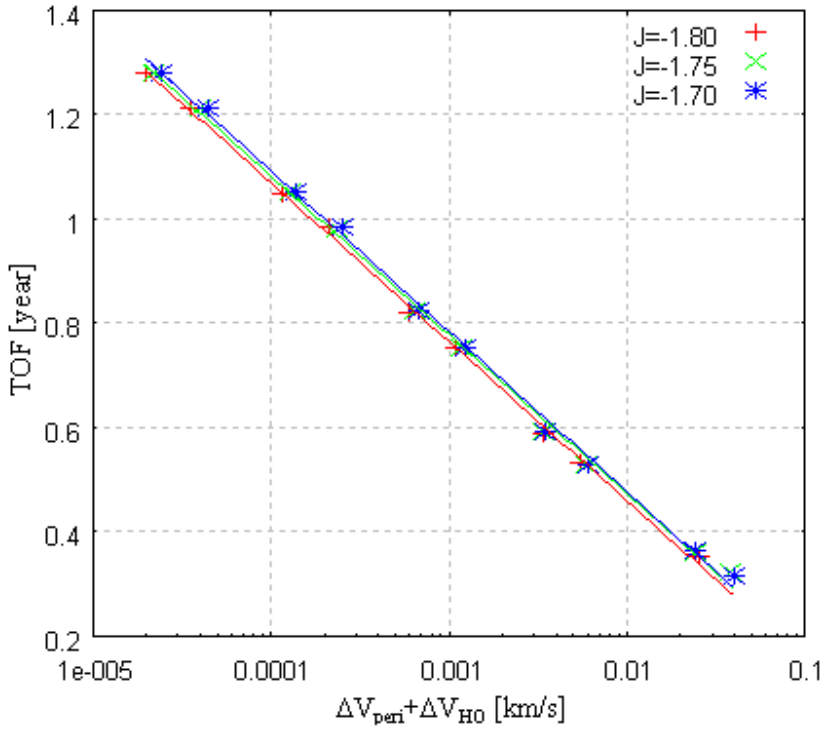

Figure 4.7: Relation between the TOF and ΔV (Changing the size of Halo orbits).

4.2 Summary

Reducing the time of flight for escape and capture trajectories between the Halo orbits and the periapsis of manifolds was discussed. By applying the ΔV_{peri} and ΔV_{HO} at the periapsis and at the point on a Halo orbit, respectively, the TOF could decrease considerably. Moreover, the relation between the TOF and log ΔV was found.

CHAPTER 5

5 Analysis of Linking Interplanetary Transfer Trajectories with the Stable and Unstable Manifolds of Halo Orbits

In this chapter, we focus on investigating the applicability of the escape and capture trajectories from/to Halo orbits to interplanetary transfer missions, using the impulsive maneuvers at the periapsis of the manifolds. We assume that the interplanetary transfer trajectories are approximated by a patched conic method. We concentrate our attention on a connection between the manifolds of the Earth Halo orbits and the manifolds of Mars Halo orbits, although these results can be applied to other planets of the solar system as well.

5.1 Interplanetary Transfer from Earth to Mars

Figure 5.1 shows a general elliptic trajectory of the Earth-Mars interplanetary transfer. The inner and outer circles correspond to Earth and Mars orbit, respectively. Symbol v_E and v_M are the Earth and Mars orbital velocities. At Earth departure hyperbolic velocity, $v_{\infty,d}$, is added to escape from the Earth, subsequently the spacecraft arrives at Mars with the arrival hyperbolic excess velocity, $v_{\infty,a}$.

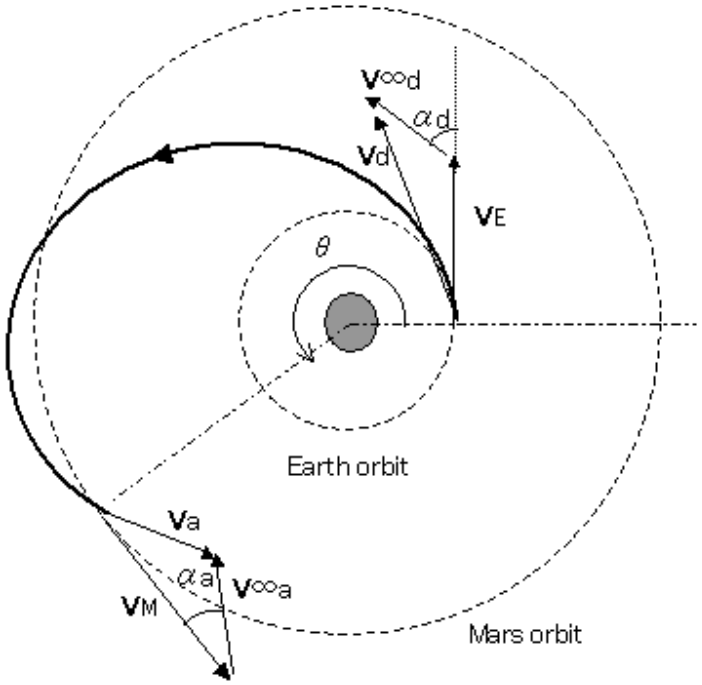

Figure 5.1: Interplanetary transfer from Earth to Mars.

5.2 Connection between Interplanetary Trajectories with Escape Trajectories

First, the location of perigee of departure hyperbolic trajectories from the Earth for interplanetary transfers is discussed in this section. That point would be used to perform escape impulsive maneuvers for transfer to Mars.

Figure 5.2 shows the periapsis of the departure hyperbola, *P*, in the ecliptic plane. A direction of the departure excess hyperbolic velocity relative to the orientation of the Earth orbital velocity vector is expressed as

$$\alpha_d = \cos^{-1}\left(\frac{\vec{v}_E \cdot \vec{v}_{\infty,d}}{|\vec{v}_E||\vec{v}_{\infty,d}|}\right) \tag{5.1}$$

We call β_d the orientation of periapsis location to the direction of $v_{\infty,d}$, which is represented by

$$\beta_d = \cos^{-1}\left(\frac{1}{1+\frac{(r_E+h)\,|\,\vec{v}_{\infty,d}\,|^2}{\mu_E}} \right) \tag{5.2}$$

where r_E and μ_E are the radius and the gravitational parameter of the Earth, respectively, and h is a perigee altitude. The value of β_d depends on the magnitude of the departure hyperbolic excess velocity if the perigee altitude is fixed. The value of phase angle α_d and β_d become zero and 29.2 deg, respectively, in the case of the Earth-Mars Hohmann transfer.

Next, the location and the velocity of the first periapsis of the Earth unstable manifolds are discussed (in view of the time of flight, only the first periapsis is discussed here.). As mentioned in chapter 3, the position and the velocity of the first periapsis of manifolds depend on the value of the Jacobi constant and whether L1 or L2 manifolds. Figure 5.3 shows an example first periapsis location of the Earth L1 and L2 unstable manifold (for J = -1.75 at the altitude h = 300 km) and each arrow indicates the direction of velocity of the Earth unstable manifolds at the first periapsis when the z component of velocity is small. Here, P_s is a periapsis of the slow escape transfer and P_f is a periapsis of the fast escape transfer. For a general spacecraft transfer from Earth to Mars, the departure hyperbolic excess velocity, $v_{\infty,d}$, is added to the direction of the Earth orbital velocity. Therefore, the Earth L1 unstable manifolds would be selected to connect with the interplanetary trajectory, rather than Earth L2 unstable manifolds.

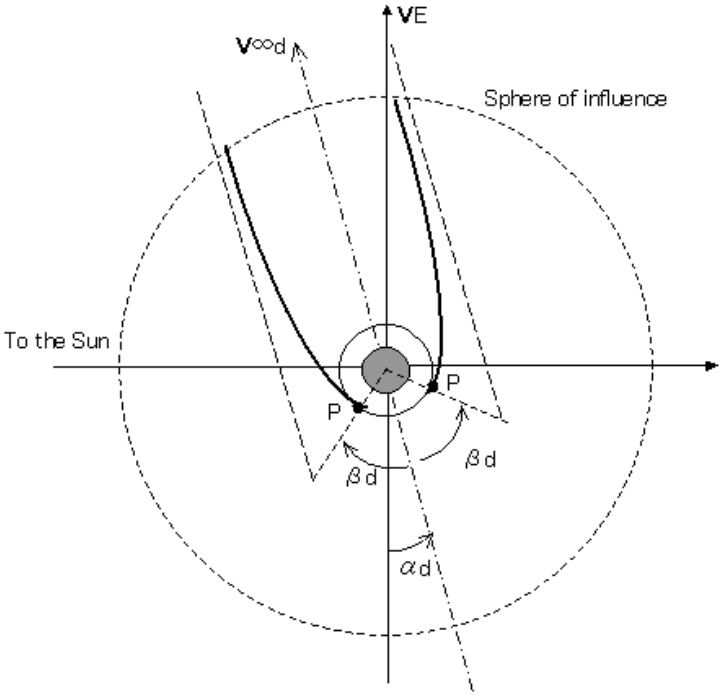

Figure 5.2: Spacecraft departure trajectory for the interplanetary transfer from Earth to Mars.

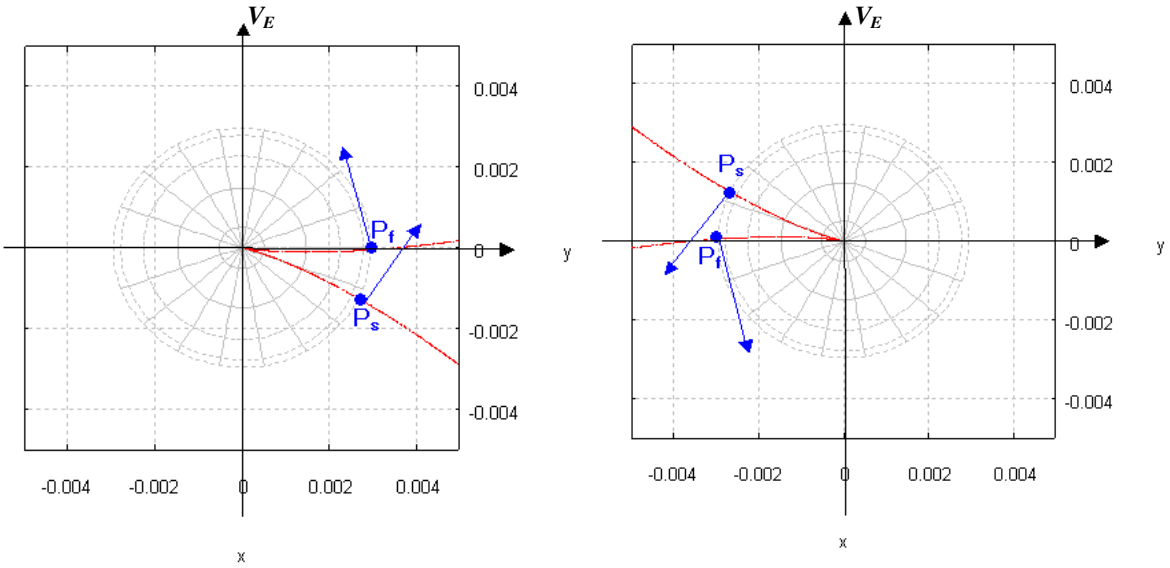

a) L1 unstable manifold **b) L2 unstable manifold**

Figure 5.3: The location of periapsis of Earth unstable manifolds in the ecliptic plane. A center circle represents the Earth.

5.3 Connection between Interplanetary Trajectories with Capture Trajectories

Next, the periapsis locations of arrival hyperbolic trajectories after an interplanetary transfer are investigated. Figure 5.4 represents a schematic diagram of the approach trajectory to Mars after the interplanetary transfer. There are two periapsis points P to Mars at an assumed altitude h = 200 km in the ecliptic plane. A phase angle α_a gives the orientation of the hyperbolic arrival velocity $v_{\infty,a}$ with respect to the direction opposite to the Mars velocity, and β_a gives the orientation of the periapsis point direction (h = 200 km) with respect to $v_{\infty,a}$. These phase angles α_a and β_a are expressed,

$$\alpha_a = \cos^{-1}\left(\frac{\vec{v}_M \cdot \vec{v}_{\infty,a}}{|\vec{v}_M||\vec{v}_{\infty,a}|}\right), \tag{5.3}$$

$$\beta_a = \cos^{-1}\left(\frac{1}{1+\frac{(r_M+h)|\vec{v}_{\infty,a}|^2}{\mu_M}}\right), \tag{5.4}$$

where r_M and μ_M are radius of Mars and gravitational parameter of the Mars, respectively. For comparison, α_a is zero and β_a is equal to 51.1 deg in the case of an Earth-Mars Hohmann transfer case.

Moreover, we study the location and the velocity of the first periapsis point of the Mars stable manifolds. Figure 5.5 shows an example first periapsis location of the Mars L1 and L2 stable manifold for J = -0.758 at the altitude h = 200 km and each arrow indicates the direction of velocity of stable manifolds at the first periapsis when the z component of velocity is small (see chapter 3). Here, P_s is a periapsis of the slow capture transfer and P_f is a periapsis of the fast capture transfer. The direction of the capture hyperbolic velocity, $v_{\infty,a}$, in the case of transfers from Earth to Mars should be in the opposite direction of the Mars velocity. Thus, the Mars "L2" stable manifold is chosen to connect with the interplanetary trajectory instead of Mars "L1" stable manifold.

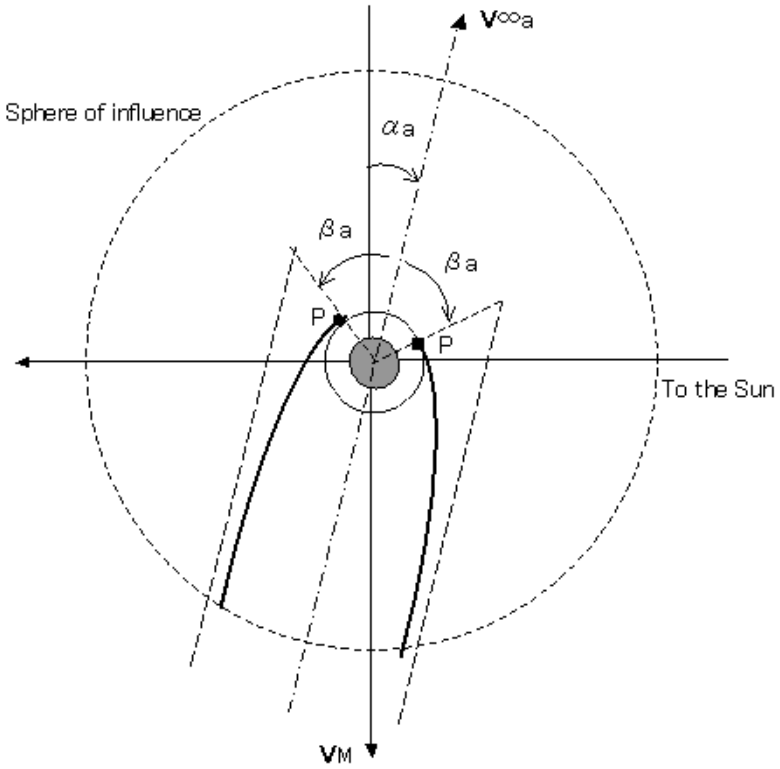

Figure 5.4: Spacecraft approach trajectory for the interplanetary transfer from Earth to Mars.

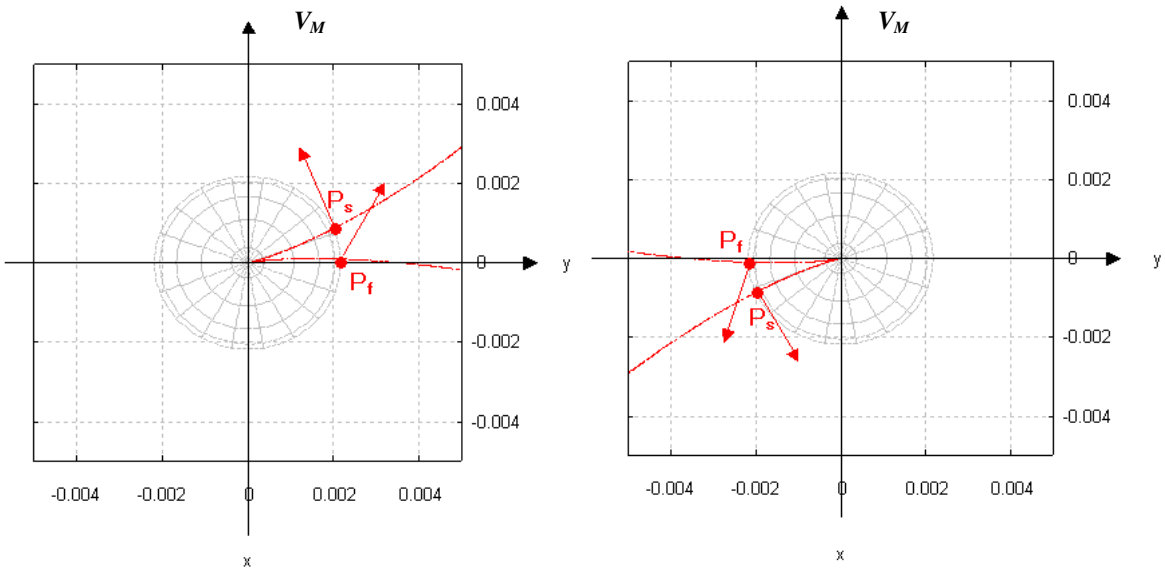

a) L1 stable manifold **b) L2 stable manifold**

Figure 5.5: The location of periapsis of stable manifold in the ecliptic plane. A center circle represents the Mars.

5.4 Interplanetary Return from Mars to Earth

For a return mission, Figure 5.6 shows a general interplanetary trajectory from Mars to Earth. The speed of the spacecraft must be reduced for it to go into the lower-energy transfer at Mars departure. Thus, the periapsis location of the departure hyperbolic trajectory from Mars to Earth is opposite to that of the transfer from Earth to Mars with respect to the origin (Figure 5.7). Therefore, the Mars L2 unstable manifold is selected to connect with the interplanetary trajectory to the Earth. On the other hand, the periapsis of the arrival hyperbolic trajectory to Earth from Mars is located like in Fig. 5.8. Hence, the Earth L1 stable manifold is chosen to connect with the interplanetary trajectory from Mars.

For these reasons, putting spaceports at Earth L1 Halo orbit and Mars L2 Halo orbit is effective from a propellant standpoint.

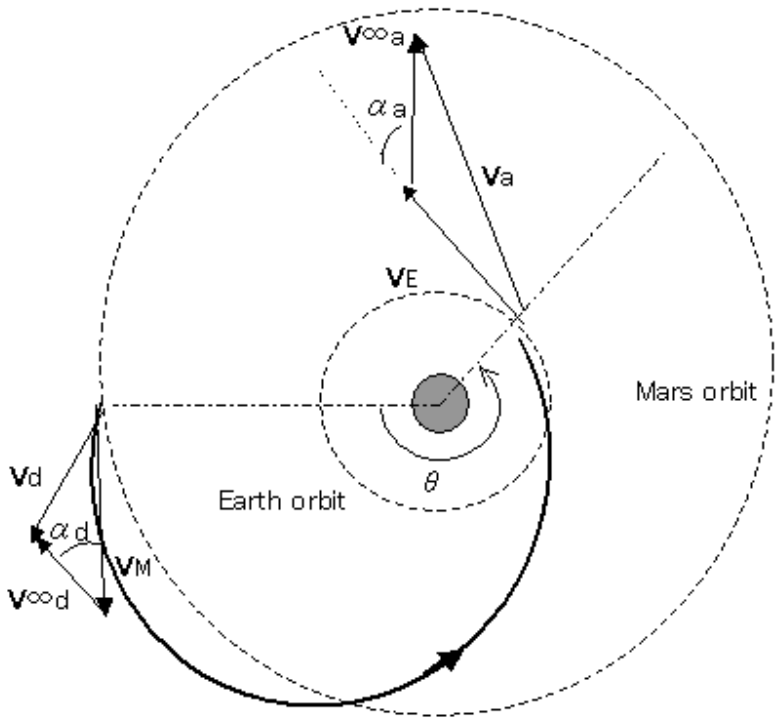

Figure 5.6: Return interplanetary transfer from Mars to Earth.

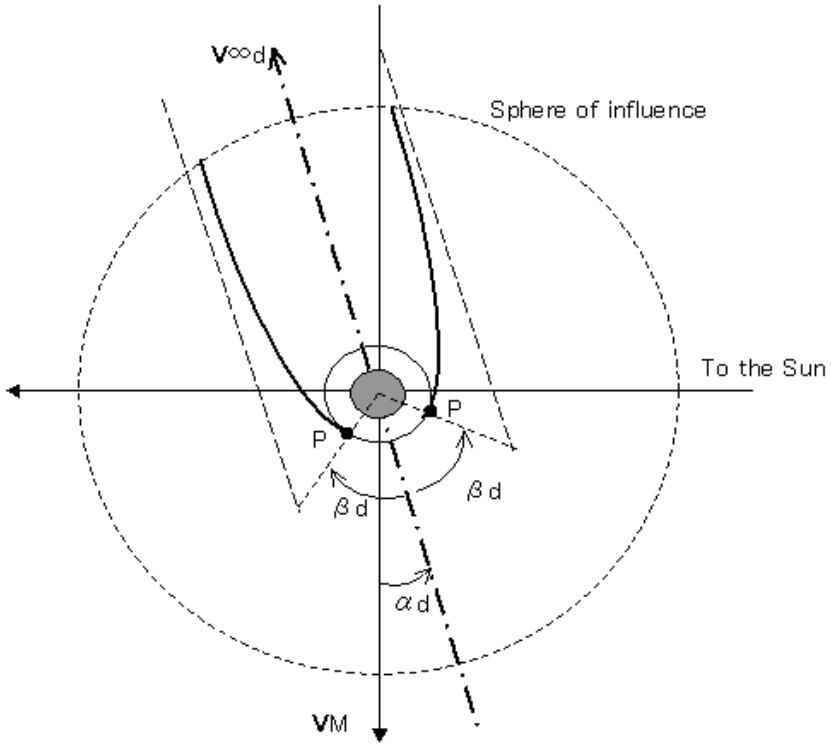

Figure 5.7: Spacecraft departure trajectory for the interplanetary transfer from Mars to Earth.

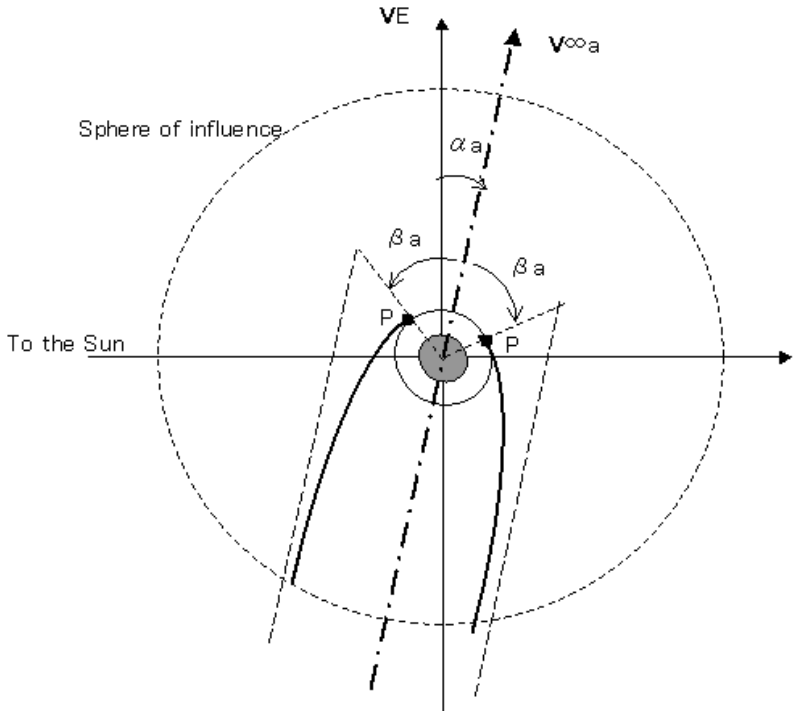

Figure 5.8: Spacecraft arrival trajectory for the interplanetary transfer from Mars to Earth.

5.5 Numerical Results in the Coplanar Circular Model Case

From here, a patched conic approximation for the interplanetary transfer is applied to our study of the escape and the capture using impulsive maneuver on Halo orbits manifolds. We focus our attention on a transfer between Earth and Mars. However, these results can be applied to other planets of the solar system as well.

First, a transfer between Earth L1 Halo orbit and Mars L2 Halo orbit is discussed using the Hill model around Earth and Mars and the coplanar circular model between the Earth and Mars. When we connect the Halo manifolds with interplanetary trajectories assuming impulsive maneuvers near the surface of planets, the position of periapsis of Halo manifolds should be matched with that of periapsis of hyperbolic trajectories. Furthermore, it is optimal when the directions of velocity coincide. Therefore, we change the position and velocity direction of periapsis of hyperbolic trajectories for interplanetary transfer by varying the interplanetary transfer angle and the flight time between Earth and Mars, and change the position and velocity directions of periapsis of Halo manifolds by varying the size of the Halo orbit. Here, the required cost for varying the size of Halo orbits is small compared to the cost for interplanetary transfers ($\Delta V \cong 40$ m/s with nearly 120 days [42]).

Tables 5.1 and 5.2 show the cost for the transfer from Earth L1 Halo orbit to Mars L2 Halo orbit. The columns called "ΔV_E_Phasing_Transfer" and "ΔV_M_Phasing_Transfer" represent maneuvers to adjust the size of Earth and Mars Halo orbits for the Earth-Mars interplanetary transfer, respectively. "ΔV_E_Halo_Depart" and "ΔV_M_Halo_Insert" indicate impulsive maneuvers to reduce the TOF of the Earth Halo escape and Mars Halo capture between periapsis of manifolds and points on Halo orbit (see chapter 4). "ΔV_E_Escape" is performed at perigee of the unstable manifold of the Earth L1 Halo orbit for the interplanetary transfer. "ΔV_M_Capture" is used at periapsis of the stable manifold for the capture to Mars L2 Halo orbit. "A_y_E" and "A_y_M" indicate y-amplitudes of the Earth and Mars Halo orbits. As a result, interplanetary trajectories between Earth Halo orbits and Mars Halo orbits with reasonable total ΔV and TOF were found. The required ΔV is less than half that of Alonso & Howell, and the TOF is about a quarter of Alonso & Howell [41]. This is because impulsive maneuvers for interplanetary transfers are assumed to be applied near the surface of planets in this study, as opposed to at deep space in the Alonso & Howell's study.

The same goes for a return transfer from Mars L2 Halo orbit to Earth L1 Halo orbit (tables 5.3 and 5.4).

Table 5.1 Required ΔV for the transfer from Earth L1 Halo to Mars L2 Halo

Type	ΔV_E Phasing Transfer	ΔV_E Halo Depart	ΔV_E Escape	ΔV_M Capture	ΔV_M Halo Insert	ΔV_M Phasing Transfer	**Total ΔV**
Coplanar circular	0.04	~ 0.09	0.82	0.91	~ 0.04	0.04	**~1.94**
Alonso [41]	2.83 (Link Earth unstable manifold to Arc)			2.45 (Link Arc to Mars stable manifold)			**5.28**

(ΔV= km/s)

Table 5.2 Required TOF for the transfer from Earth L1 Halo to Mars L2 Halo

Type	TOF Phasing Transfer	TOF E.Halo ~ E.Peri	TOF E.Peri ~ M.Peri	TOF M.Peri ~ M.Halo	TOF Phasing Transfer	**Total TOF**	A_y_E	A_y_M
Coplanar circular	120	69	308	117	120	**734**	0.755	0.552
Alonso [41]			2919			**2919**	-	**-**

(TOF = days)

Table 5.3 Required ΔV for the return transfer from Mars L2 Halo to Earth L1 Halo

Type	ΔV_E Phasing Transfer	ΔV_E Halo Insert	ΔV_E Capture	ΔV_M Escape	ΔV_M Halo Depart	ΔV_M Phasing Transfer	**Total ΔV**
Coplanar circular	0.04	~ 0.09	0.82	0.91	~ 0.04	0.04	**~1.94**

(ΔV= km/s)

Table 5.4 Required TOF for the return transfer from Mars L2 Halo to Earth L1 Halo

Type	TOF Phasing Transfer	TOF E.Halo ~ E.Peri	TOF E.Peri ~ M.Peri	TOF M.Peri ~ M.Halo	TOF Phasing Transfer	**Total TOF**	A_y_E	A_y_M
Coplanar circular	120	69	308	117	120	**734**	0.755	0.552

(TOF = days, A_y = million km)

5.6 Numerical Results in the Ephemeris Model Case

Next, a transfer between Earth L1 Halo orbit and Mars L2 Halo orbit is discussed in the Hill three-body model around the Earth and Mars and in the real Ephemeris model between Earth sphere and Mars sphere. In a manner similar to the simple ephemeris model case, we investigate a solution to connect the Earth and Mars Halo manifolds with interplanetary trajectories by varying the departure and arrival dates from/to Earth and Mars, and by varying the size of the Earth and Mars Halo orbits, assuming impulsive maneuvers near the surface of planets.

Tables 5.5 - 5.8 show the ΔV and the TOF for the transfer from Earth L1 Halo orbit to Mars L2 Halo orbits, and for the return transfer from Mars L2 Halo orbits to Earth L1 Halo orbits using the Ephemeris data for a time interval between 2009 and 2015. It was found that Earth L1 Halo and Mars L2 Halo orbit could be connected at the reasonable ΔV and TOF as in the case of previous coplanar circular model case, but those values differ by about 10 % since Earth and Mars orbits are not circular.

Table 5.5 Required ΔV for the transfer from Earth L1 Halo to Mars L2 Halo

Departure & Arrival date	ΔV_E Phasing Transfer	ΔV_E Halo Depart	ΔV_E Escape	ΔV_M Capture	ΔV_M Halo Insert	ΔV_M Phasing Transfer	**Total ΔV**
Sep. 2009 ~ Oct. 2010	0.04	0.09	0.88	0.93	0.04	0.04	**2.02**
Oct. 2011 ~ Oct. 2012	0.04	0.06	0.69	1.01	0.04	0.04	**1.88**
Nov. 2013 ~ Oct. 2014	0.04	0.06	0.56	1.10	0.04	0.04	**1.84**

(ΔV= km/s)

Table 5.6 Required TOF for the transfer from Earth L1 Halo to Mars L2 Halo

Departure & Arrival date	TOF Phasing Transfer	TOF E.Halo ~ E.Peri	TOF E.Peri ~ M.Peri	TOF M.Peri ~ M.Halo	TOF Phasing Transfer	**Total TOF**	A_y_E	A_y_M
Sep. 2009 ~ Oct. 2010	120	62	384	117	120	**803**	0.743	0.571
Oct. 2011 ~ Oct. 2012	120	69	356	117	120	**782**	0.729	0.558
Nov. 2013 ~ Oct. 2014	120	69	318	117	120	**744**	0.739	0.547

(TOF = days, A_y = million km)

Table 5.7 Required ΔV for the return transfer from Mars L2 Halo to Earth L1 Halo

Departure & Arrival date	ΔV_E Phasing Transfer	ΔV_E Halo Insert	ΔV_E Capture	ΔV_M Escape	ΔV_M Halo Depart	ΔV_M Phasing Transfer	**Total ΔV**
Jul. 2011~Jul. 2012	0.04	0.09	0.93	0.87	0.04	0.04	**2.01**
Aug. 2013~Aug. 2014	0.04	0.09	0.84	1.11	0.04	0.04	**2.16**
Oct. 2015~Sep. 2016	0.04	0.09	0.76	1.37	0.04	0.04	**2.34**

(ΔV= km/s)

Table 5.8 Required TOF for the return transfer from Mars L2 Halo to Earth L1 Halo

Departure & Arrival date	TOF Phasing Transfer	TOF E.Halo ~ E.Peri	TOF M.Peri ~ E.Peri	TOF M.Peri ~ M.Halo	TOF Phasing Transfer	**Total TOF**	A_y_E	A_y_M
Jul. 2011 ~ Jul. 2012	120	62	380	117	120	**799**	0.758	0.578
Aug. 2013 ~ Aug. 2014	120	62	390	117	120	**809**	0.789	0.584
Oct. 2015 ~ Sep. 2016	120	62	361	117	120	**780**	0.817	0.576

(TOF = days, A_y = million km)

5.7 Summary

Connection strategies between the manifolds of the Earth Halo orbits and the manifolds of Mars Halo orbits were discussed. The periapsis values of the departure and the arrival hyperbolic trajectories for the interplanetary transfers were investigated. Moreover, the characteristics of the periapsis of the stable and unstable manifolds associated with Earth and Mars Halo orbits were also examined. From these results, a connection between the Earth L1 manifold and the Mars L2 manifold was feasible and preferable from a propellant viewpoint.

Furthermore, the required total ΔV and the TOF for the transfer between Earth L1 Halo orbits and Mars L2 Halo orbits were investigated in the simple and real ephemeris model by varying the departure and arrival date from/to Earth and Mars, and by varying the size of the Earth and Mars Halo orbits. It was found that that Earth L1 Halo and Mars L2 Halo orbits could be connected at a reasonable ΔV and TOF.

CHAPTER 6

6 Application to Earth-Mars Transportation System

6.1 Application to Earth-Mars Transportation System using Spaceports at Halo Orbits

In this section, an application to Earth-Mars transportation system, between low earth orbits (LEO) and low mars orbits (LMO), using spaceports at Earth and Mars Halo orbit is discussed and compared with a direct transfer system.

Tables 6.1 and 6.2 show the required ΔV and TOF for a transfer between LEO (altitude = 300 km) and LMO (altitude = 200 km) via the Earth and Mars Halo orbits and for a direct transfer case using ephemeris data from 2009 to 2016. "ΔV_LEO" and "ΔV_LMO" are maneuvers for a transfer from LEO to Earth Halo orbit and from Mars Halo orbit to LMO, respectively. "ΔV_E_Halo_Insert" and "ΔV_E_Halo_Insert" are performed to reduce TOF between LEO/LMO and Earth/Mars Halo orbit, and "ΔV_E_Phasing_LEO" and "ΔV_M_Phasing_LMO" indicate phasing maneuvers to adjust the size of the Earth and Mars Halo orbits for transfers between LEO/LMO and Earth/Mars Halo orbits. For maneuvers No. 4 ~ 9, refer to Section 5.5. It was found that the required total ΔV for a transfer from LEO to LMO via Earth and Mars Halo orbits is slightly greater than that of the direct transfer, and the TOF is longer. The same could be said for return transfers from the LMO to LEO via Mars and Earth Halo orbits as shown in Tables 6.3 and 6.4. From these results, the system using Halo orbits has no advantage over the direct transfer with respect to ΔV and TOF. However, the system using Halo orbits is evaluated from a different standpoint next section.

Considering the round-trip transfer between LEO and LMO, phasing maneuvers to adjust the size of Earth and Mars Halo orbits for return interplanetary transfers ("ΔV_E.Phasing_transfer" and "ΔV_M.Phasing_transfer") are as small as mentioned before [42]. On the other hand, phasing maneuver to adjust the phase of LMO for return interplanetary transfers could be large (see Appendix).

Table 6.1 Required ΔV for the transfer from LEO to LMO

Maneuver No. (No. for direct)	1	2	3	4	5	6 (i)	7 (ii)	8	9	10	11	12	
Transfer type (Departure date from LEO)	ΔV LEO	ΔV_E Halo Insert	ΔV_E Phasing LEO	ΔV_E Phasing Transfer	ΔV_E Halo Depart	ΔV_E Escape	ΔV_M Capture	ΔV_M Halo Insert	ΔV_M Phasing Transfer	ΔV_M Phasing LMO	ΔV_M Halo Depart	ΔV LMO	**Total ΔV**
Via Halo (in 2009)	3.15	0.06	0.04	0.04	0.09	0.88	0.93	0.04	0.04	0.04	0.04	1.42	**6.79**
Direct (in 2009)	-	-	-	(0~5.0)	-	3.67	2.03	-	(0~2.0)	-	-	-	**5.70 (~12.70)**
Via Halo (in 2011)	3.15	0.06	0.04	0.04	0.06	0.69	1.01	0.04	0.04	0.04	0.04	1.42	**6.62**
Direct (in 2011)	-	-	-	(0~5.0)	-	3.63	2.16	-	(0~2.0)	-	-	-	**5.79 (~12.79)**
Via Halo (in 2013)	3.15	0.06	0.04	0.04	0.06	0.56	1.10	0.04	0.04	0.04	0.04	1.42	**6.59**
Direct (in 2013)	-	-	-	(0~5.0)	-	3.64	2.39	-	(0~2.0)	-	-	-	**6.03 (~13.03)**

(ΔV= km/s)

Table 6.2 Required TOF for the transfer from LEO to LMO

Transfer type (Departure date from LEO)	TOF LEO ~ E.Halo	TOF E.Phasing LEO	TOF E.Phasing Transfer	TOF E.Halo ~ E.peri	TOF E.peri ~ M.peri	TOF M.Peri ~ M.Halo	TOF M.Phasing Transfer	TOF M.Phasing LMO	TOF M.Halo ~ LMO	**Total TOF**
Via Halo (in 2009)	69	120	120	62	384	117	120	120	117	**1226**
Direct (in 2009)	-	-	-	-	322	-	-	-	-	**322**
Via Halo (in 2011)	69	120	120	69	356	117	120	120	117	**1208**
Direct (in 2011)	-	-	-	-	307	-	-	-	-	**307**
Via Halo (in 2013)	69	120	120	69	318	117	120	120	117	**1170**
Direct (in 2013)	-	-	-	-	294	-	-	-	-	**294**

(TOF = days)

Table 6.3 Required ΔV for the return transfer from LMO to LEO

Maneuvers No. (No. for direct)	24	23	22	21	20	19 (iv)	18 (iii)	17	16	15	14	13	
Transfer type (Departure date from LMO)	ΔV LEO	ΔV_E Halo Depart	ΔV_E Phasing LEO	ΔV_E Phasing Transfer	ΔV_E Halo Insert	ΔV_E Capture	ΔV_M Escape	ΔV_M Halo Depart	ΔV_M Phasing Transfer	ΔV_M Phasing LMO	ΔV_M Halo Insert	ΔV LMO	**Total ΔV**
Via Halo (in 2011)	3.15	0.06	0.04	0.04	0.09	0.93	0.87	0.04	0.04	0.04	0.04	1.42	**6.76**
Direct (in 2011)	-	-	-	(0~5.0)	-	3.64	2.07	-	(0~2.0)	-	-	-	**5.71 (~12.71)**
Via Halo (in 2013)	3.15	0.06	0.04	0.04	0.09	0.84	1.11	0.04	0.04	0.04	0.04	1.42	**6.91**
Direct (in 2013)	-	-	-	(0~5.0)	-	3.79	2.06	-	(0~2.0)	-	-	-	**5.85 (~12.85)**
Via Halo (in 2015)	3.15	0.06	0.04	0.04	0.09	0.76	1.37	0.04	0.04	0.04	0.04	1.42	**7.09**
Direct (in 2015)	-	-	-	(0~5.0)	-	3.98	2.06	-	(0~2.0)	-	-	-	**6.04 (~13.04)**

(ΔV= km/s)

Table 6.4 Required TOF for the return transfer from LMO to LEO

Transfer type (Departure date from LMO)	TOF LEO ~ E.Halo	TOF E.Phasing LEO	TOF E.Phasing Transfer	TOF E.Halo ~ E.peri	TOF E.peri ~ M.peri	TOF M.Peri ~ M.Halo	TOF M.Phasing Transfer	TOF M.Phasing LMO	TOF M.Halo ~ LMO	**Total TOF**
Via Halo (in 2011)	69	120	120	62	380	117	120	120	117	**1225**
Direct (in 2011)	-	-	-	-	329	-	-	-	-	**329**
Via Halo (in 2013)	69	120	120	62	390	117	120	120	117	**1235**
Direct (in 2013)	-	-	-	-	350	-	-	-	-	**350**
Via Halo (in 2015)	69	120	120	62	361	117	120	120	117	**1206**
Direct (in 2015)	-	-	-	-	229	-	-	-	-	**229**

(TOF = days)

6.2 Evaluation of the Earth-Mars Transportation System using Halo Orbits

The Earth-Mars transportation system using spaceports at Earth and Mars Halo orbits is evaluated by the spacecraft mass for the round-trip transfer. Table 6.5 shows the required wet mass for the round-trip transfer that starts from LEO in 2013. Here, we assume the following things:

- Payload mass carried during round-trip transfer is unit.
- The specific impulse (Isp) of spacecraft is 300 seconds.
- Structure and bus mass is 4 times heavier than the payload mass.
- The propellant for return from Earth Halo orbits to LEO is left at spaceport on Earth Halo orbits on the way to LMO.
- The propellant for return from Mars Halo orbits to Earth Halo orbits is left at spaceport on Mars Halo orbits on the way to LMO.

From Table 6.5, compared with direct transfer between LEO and LMO, it is shown that the mass of the Earth-Mars transportation system S/C is reduced by half when starting from LEO using spaceports on Earth and Mars Halo orbits to leave propellant for the return transfer. The reason is simply because it is not necessary to carry the whole propellant for the return to LMO. First, the propellant for returning from Earth Halo orbits to LEO (10.1) is left at the spaceport on Earth Halo orbits. And then, the propellant necessary for returning from the Mars Halo orbit to the Earth Halo orbit (6.1) is left at the spaceport on Mars Halo orbits Consequently, the propellant for the transfer from LMO to Mars Halo orbit (3.3) should be only carried to LMO. Therefore, it can be concluded that this round-trip transportation system using spaceport at the Earth and Mars Halo orbits is effective. For comparison, Fig 6.1 shows the wet mass (the dry mass and the required propellant mass) starting from LEO in the case of nonleaving propellant at neither of spaceports, the case of leaving propellant at only the Earth spaceport, the case of leaving propellant at both Earth and Mars spaceports, and the case of direct transfer. Numbers in figure (1 ~ 24 and i ~ iv) correspond to the maneuver number in tables 6.1 and 6.3. We can say that the leaving propellant at both the Earth and Mars spaceports is the best strategy.

Table 6.5 Required mass for the round-trip transfer between LEO and LMO (Departure date from LEO in 2013 & Departure date from LMO in 2015)

Type		Via Earth and Mars Halo orbits to leave propellant for return transfer						Direct
Section		LEO ~ E.Halo	E.Halo ~ M.Halo	M.Halo ~ LMO	LMO ~ M.Halo	M.Halo ~ E.Halo	E.Halo ~ LEO	LEO ~ LMO
ΔV [km/s]		3.25	1.84	1.50	1.50	2.34	3.25	12.07~
Propellant ratio		0.669	0.465	0.399	0.399	0.548	0.669	0.983~
Dry mass	Payload mass	1	1	1	1	1	1	1
	Structure & bus mass…	4	4	4	4	4	4	4
	Carried propellant mass	42.3 (b+c+d+e+f)	14.9 (c+d+e)	3.3 (d)	0	0	0	0
Consumed propellant mass		95.6 (a)	17.3 (b)	5.5 (c)	3.3 (d)	6.1 (e)	10.1 (f)	289.1~
Wet mass		**142.9**	37.2	13.8	8.3	11.1	15.1	**294.1~**

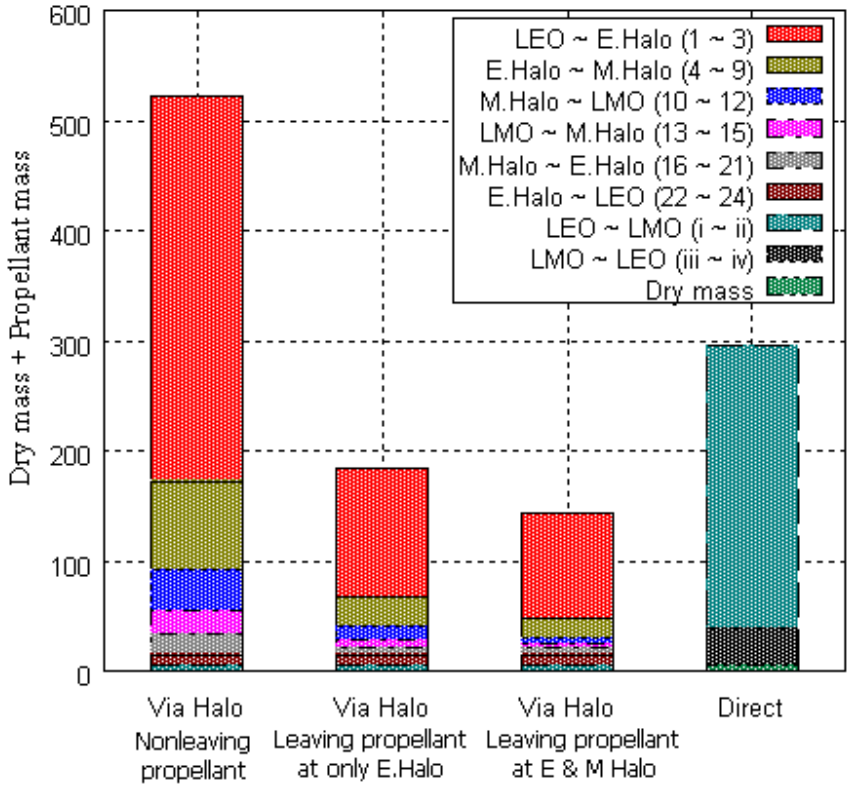

Fig. 6.1: Dry mass and propellant mass

6.3 Application to Interplanetary Transfers other than Mars

For transfers to outbound targets such as Mars, the Earth spaceport is needed to be located on Earth "L1" Halo orbit. However, for transfers to inbound targets such as Venus, the Earth spaceport is needed to be located on Earth "L2" Halo orbit. Heteroclinic orbits utilized in the Genesis mission (Fig. 6.2 [7]) could be used to move the Earth spaceport between L1 Halo orbits and L2 Halo orbits ($\Delta V \cong 10$ m/s & TOF $\cong 0.4$ years).

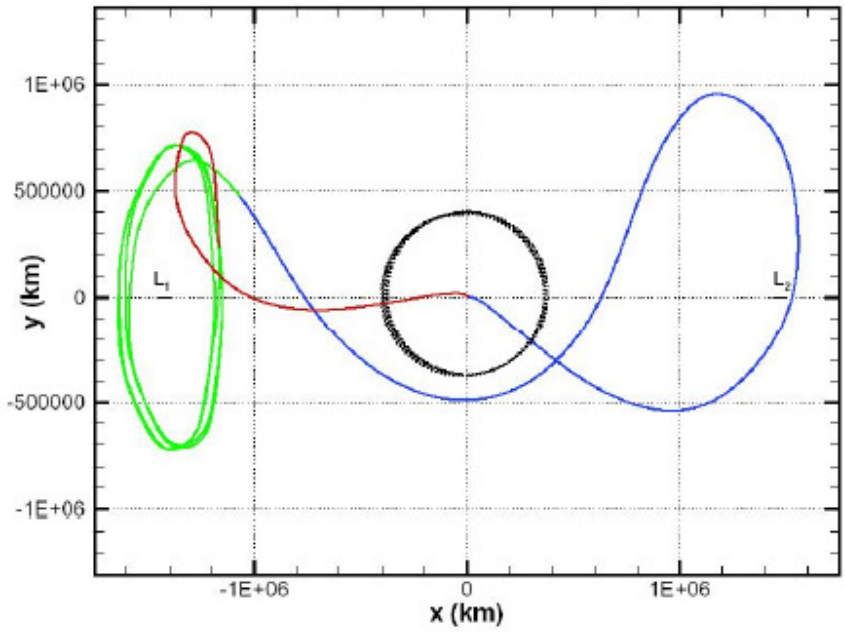

Fig. 6.2: Genesis trajectory [7]

6.4 Summary

Application to Earth-Mars transportation system putting spaceports at Earth and Mars Halo orbits was investigated. It was found that the required total ΔV for a transfer between LEO and LMO via Earth and Mars Halo orbits is slightly larger than that of the direct transfer, and the TOF becomes longer. However, by considering the round-trip transfer between LEO and LMO, the system using spaceports in Earth and Mars Halo orbits to leave propellant for the return transfer is useful compared to the direct transfer.

CHAPTER 7

7 Conclusions

This dissertation discussed the escape and the capture trajectories from/to Halo orbits using impulsive maneuvers at periapsis of the manifold for interplanetary transfers, and proposed for application to the Earth-Mars round-trip transportation system.

First, the characteristics of periapsis of Halo orbit manifolds were investigated. The relations between the minimum periapsis distance of the manifold trajectories and the size of the Halo orbits were obtained. As a result, the manifold trajectories of the periapsis passage points from Halo orbits can intersect the surface of any of the planets in the solar system by adjusting the size of the Halo orbits. Therefore, the impulsive maneuver for the interplanetary transfer could be used near the surface of planets on the manifolds of Halo orbits.

Second, the reduction of the TOF for the escape and capture from/to Halo orbits was studied. It was found that a little velocity correction (around 0.06 km/s) could decrease the TOF by more than a year.

Next, the links between interplanetary trajectory and escape/capture trajectories from/to Halo orbits were analyzed. The survey found existing interplanetary trajectories between Earth L1 Halo orbit and Mars L2 Halo orbits with reasonable delta-V and flight time.

Finally, our strategy is applied to the Earth-Mars transportation system. The required delta-V for the round-trip transfer between LEO and LMO via spaceports on Earth and Mars Halo orbits becomes slightly larger than that of the direct round-trip transfer. However, in an evaluation in terms of the required spacecraft wet mass of the Earth-Mars transportation system putting spaceports at Halo orbits, the wet mass starting from LEO could be reduced by half compared to the direct transfer by leaving propellant for return at spaceports at the Earth and Mars Halo orbits on the way to LMO.

Bibliography

1. D' Amario, L. A., and Edelbaum, T. N., "Minimum Impulse Three-Body Trajectories," *AIAA Journal*, Vol. 12, No. 4, 1974, pp. 455-462.

2. Broucke, R., "Travelling Between the Lagrange Points and the Moon," *Journal of Guidance and Control*, Vol. 2, No. 4, 1979, pp. 257-263.

3. Gomez, G., Jorba, A., Masdemont, J. and Simo, C., "Study of the Transfer from the Earth to a Halo Orbit Around the Equilibrum Point L1," *Celestial Mechanics and Dynamical Astronomy*, Vol. 56, No. 4, 1993, pp. 541-562.

4. Prado, A. F. B. A., "Travelling Between the Lagrange Points and the Earth," *Acta Astronautica*, Vol. 39, No. 7, 1996, pp. 483-486.

5. J.D. Strizzi, J. Kutrieb, P. Damphousse, J. Carrico, "Sun-Mars Libration Points and Mars Mission. Simulations," AAS 01-159, AAS/AIAA Spaceflight Mechanics Meeting, Santa Barbara, California, USA,. February 2001

6. Baoyin, H., McInnes, R. C., "Trajectories to and from the Lagrange points and the primary body surfaces," *Journal of Guidance, Control, and Dynamics*, Vol. 29, No. 4., 2006, pp 998-1003.

7. Canalias, E., Gomez, G., Marcote, M., and Masdemont, J. J., "Assessment of Mission Design Including Utilization of Libration Points and Weak Stability Boundaries," *ESA Advanced Concept Team*, URL: http://www.esa.int/act.

8. Folta, D. C., et al., "Servicing and Deployment of National Resources in Sun-Earth. Libration-Point Orbits," IAC Paper 02-Q.6.08, October 2002.

9. Lo, M., and Ross, S., "The Lunar L1 Gateway: Portal to the Stars and Beyond," AIAA Paper 2001-4768, August 2001.

10. J.E. Marsden & S.D. Ross, "New Methods in Celestial Mechanics and Mission Design," Bulletin of the American Mathematical Society, Vol. 43, No. 1, pp. 43-73, 2006.

11. Farquhar, R. W., "Future Missions for Libration-Point Satellites," *Astronautics and Aeronautics*, Vol. 7, No. 5, May 1969, pp. 52-56.

12. Farquhar, R W., Dunham D W., Guo, Yan-ping and Madams, V. J., "Utilization of libration points for human exploration in the sun-earth-moon system and beyond, " *Acta Astronautica*, Vol. 55, pp. 687-700, 2004.

13. Website: "JAXA Vision - JAXA 2005 -," URL: http://www.jaxa.jp/2025/index_e.html.

14. Conley, C.C., "Low energy transit in the restricted three body problem," *SIAM Journal on Applied Mathematics*, Vol. 16, No. 4, pp. 732-746, 1968.

15. Koon, W. S., Lo, M. W., Marsden, J. E. & Ross, S. D. "Heteroclinic Connections Between Periodic Orbits and Resonance Transitions in Celestial Mechanics," *Chaos*, Vol. 10, No. 2, 2000, pp. 427-469.

16. Koon, W. S., Lo, M. W., Marsden, J. E. & Ross, S. D., "Constructing a Low Energy Transfer Between Jovian Moons Contemp," *Contemporary Mathematics*, Vol., 292, 2002, pp. 129-145.

17. Lo, M. “The Interplanetary Superhighway and the Origins Program”, IEEE Space 2002 Conference, Big Sky, MT, March. 2002.

18. Yamato, H. & Spencer, D. B., “Transit-Orbit Search for Planar Restricted Three-Body Problems with Perturbations.,” *Journal of Guidance, Control, and Dynamics*, Vol. 27, No. 6, pp. 1035-1045, 2004.

19. Topputo F., Vasile M., Bernelli-Zazzera F., “Low Energy Interplanetary Transfers Exploiting Invariant Manifolds of the Restricted Three Body Problem,” *Journal of the Astronautical Sciences*, 2005, Vol. 53, Number 4,pp 353-372.

20. Howell, K., and Kakoi, M., “Transfers between the Earth-Moon and Sun-Earth systems using manifolds and transit orbits,” *Acta Astronautica*, Vol. 59, pp. 367-380, 2006.

21. Matsumoto, M., and Kawaguchi, J., “Deep Space Quay and Solar Voyage Era,” *The Sixth IAA International Conference on Low-Cost Planetary Missions*, Kyoto, Japan, 11-13 October, 2005, pp. 401-408.

22. Nakamiya, M., and Yamakawa, H., “Analysis of Earth Escape Trajectories Starting from Sun-Earth L2 Point,” *16th Workshop on Astrodynamics and Flight Mechanics*, ISAS, 1-2 August 2006.

23. Nakamiya, M., and Yamakawa, H., “Earth Escape Trajectories Starting from L2 Point,” *AIAA/AAS Astrodynamics Specialist Conference and Exhibit*, Keystone, Colorado, Aug. 21-24, 2006.

24. Belbruno, E. & Miller, J., “Sun-Perturbed Earth-to-Moon Transfers with Ballistic Capture,” *Journal of Guidance, Control, and Dynamics*, Vol. 16, No. 4, 1993, pp. 770-775.

25. Yamakawa, H., Kawaguchi, J., Ishii, N., and Matsuo, H., “On Earth-Moon Transfer Trajectory with Gravitational Capture,” *American Astronautical Society*, Paper AAS 93-633, Aug. 1993.

26. Brunini, A., “On the satellite capture problem Capture and stability regions for planetary satellites,” *Celestial Mechanics and Dynamical Astronomy*, Vol. 64, pp. 79-92, 1996.

27. Howell, K. C., Marchand, B. G. & Lo, M. W., “Temporary Satellite Capture of Short-Period Jupiter Family Comets from the Perspective of Dynamical Systems,” *Journal of the Astronautical Sciences*, Vol. 49, No. 4, pp. 539-557, 2001.

28. Zoltán Makó1 and Ferenc Szenkovits, “Capture in the circular and elliptic restricted three-body problem,” *Celestial Mechanics and Dynamical Astronomy*, Vol. 90, No. 1-2, pp. 51-58, 2004.

29. Paskowitz, M. E., and Scheeres, D. J., “Robust Capture and Transfer Trajectories for Planetary Satellite Orbiters,” *Journal of Guidance, Control, and Dynamics*, Vol. 29, No. 2., 2006, pp. 342-353

30. Scheeres, D., Guman, M., and Villac, B., “Stability Analysis of Planetary Satellite Orbiters:. Application to the Europa Orbiter,” *Journal of Guidance, Control and Dynamics*, Vol. 24, No. 4,. 2001, pp. 778–787.

31. Szebehely, V., *Theory of Orbits: The Restricted Problem of Three Bodies*, Academic Press, New York, 1967.

32. Villac, B. F. & Scheeres, D. J., “Escaping Trajectories in the Hill Three-Body Problem and Applications,” *Journal of Guidance, Control, and Dynamics*, Vol. 26, No. 2., 2003, pp. 224-232.

33. Henon, M., “Numerical exploration of the restricted problem. V,” *Astronomy and Astrophysics 1*, pp. 223–238, 1969.

34. Breakwell, J. V., and Brown, J. V., "The `Halo' Family of 3-Dimensional Periodic Orbits in the Earth-Moon' Restricted 3-Body Problem," *Celestial Mechanics*, Vol. 20, Nov. 1979, pp. 389-404.

35. Farquhar, R. W., "The Control and Use of Libration-Point Satellites," NASA Technical Report, R-346, 1970

36. Richardson, D. L., "Analytic Construction of Periodic Orbits About the Collinear Points," *Celestial Mechanics*, Vol. 22, Oct. 1980, pp. 241-253.

37. Howell, K. C., "Families of Orbits in the Vicinity of the Collinear Libration Points," *Journal of the Astronautical Sciences*, Vol. 49, No. 1, Jan.-March 2001, pp. 107-125.

38. Simo, C., and Stuchi, T., "Central Stable/Unstable Manifolds and the Destruction of KAM Tori in the Planar Hill Problem," *Physica D*, 140, pp. 1-32, 2000.

39. Gomez, G., Marcote, G., and Mondelo, J., "The Invariant Manifold Structure of the Spatial Hill's Problem," *Dynamical Systems: An International Journal*, 20 (1) 115-147, 2005.

40. Lawrence, C., Zhou, J., and Tits, A., "User's Guide for CFSQP Version 2.5: A C Code for Solving (Large Scale) Constrained Nonlinear (Minimax) Optimization Problems, Generating Iterates Satisfying All Inequality Constraints," *Institute for Systems Research, University of Maryland, Technical Report TR-94-16r1*, College Park, MD 20742, 1997.

41. Alonso, G., and Howell, K., "The design of system-to-system transfer arcs using invariant manifolds in the multi-body problem," PhD Dissertation, Purdue University, December 2006.

42. Hiday, L.A., and Howell, K.C., "Impulsive Time-Free Transfers Between Halo Orbits," *AIAA/AAS Astrodynamics Conference*, Hilton Head Island, South Carolina, August 1992.

43. Patterson, C., and Howell, K., "Representations of Invariant Manifolds for Applications in System-to-System Transfer Design," M.S. Thesis, Purdue University, December 2005.

44. Guckenheimer, J., and Holmes, P., *Nonlinear Oscillations, Dynamical Systems, and Bifurcations of Vector Fields*, Springer-Verlag, New York, 1983.

Appendix

A. Phasing Maneuvers of LEO/LMO for Interplanetary Transfer

Considering the round-trip transfer between LEO and LMO, phasing maneuvers of LEO/LMO for interplanetary transfers are required. The ΔV for phasing maneuver of LMO depends on the entry angle into LMO from LEO. For instance, a magnitude of phasing maneuvers for interplanetary transfer to LEO starting from LMO in December 2015, with the insertion into LMO in September 2014 from LEO, increases from zero to about 2.0 km/s, considering only solar perturbation. In Fig. A.1, we represent a LMO that a spacecraft is injected into with the insertion of zero degree in September 2014 from LEO, a LMO in December 2015 assuming only solar perturbations starting in September 2014, and a LMO after phasing maneuvers for interplanetary transfer to LEO starting from LMO in December 2015.

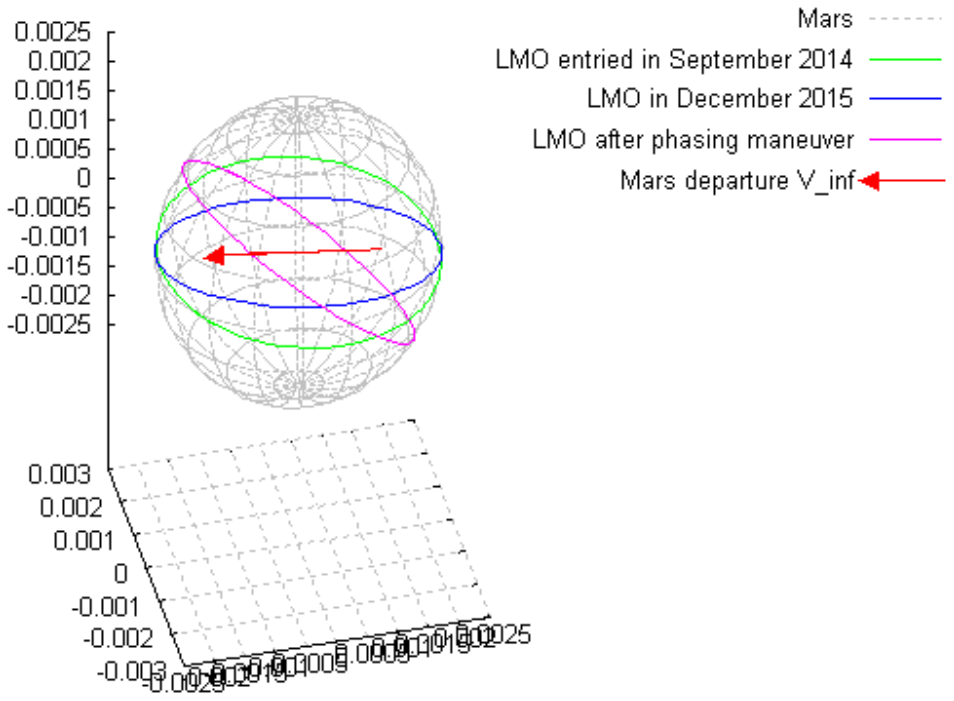

Figure A.1: LMO before and after phasing maneuver in the Sun-Mars line fixed rotating frame.